The mitochondrial splicing factor PPR9 encoded by the *AT1G03560* gene-locus is essential for the maturation of several *nad* transcripts in Arabidopsis plants

Ella Kobaivanov[1,#], Marketa Kitel[1,#], Roei Matan[1], Ron Mizrahi[1], Noa Carmi[1], Oren Ostersetzer-Biran[1,*]

[1] Department of Plant and Environmental Sciences, The Alexander Silberman Institute of Life Sciences, The Hebrew University of Jerusalem, Jerusalem, Israel

[#] These authors contributed equally to this work

Running title: PPR9 controls *nad2* and *nad7* mt-RNA splicing and CI biogenesis

*corresponding author: *e-mail* - oren.ostersetzer@mail.huji.ac.il**;** ORCID https://orcid.org/0000-0003-2197-7729

Summery

Mitochondrial biogenesis in plants relies on the transcription and proper processing of primary organellar transcripts into functional mature RNAs. This includes the removal of numerous group II-type introns, most of which reside within genes encoding subunits of respiratory complex I (CI). The maturation of mitochondrial transcripts (mt-RNAs) requires the coordinated action of numerous nuclear-encoded RNA-binding cofactors, such as maturases, RNA helicases, and members of the pentatricopeptide repeat (PPR) protein family. In this study, we characterize PPR9 (At1g03560), a mitochondrial P-type PPR protein identified in genetic screens for essential protein cofactors. Loss of PPR9 function disrupts embryogenesis, resulting in early arrest of seed development. Nevertheless, homozygous mutant plants can be maintained using an embryo-rescue approach optimized in our laboratory. Homozygous *ppr9* mutants exhibit delayed germination, retarded growth, and impaired mitochondrial respiration. Molecular analyses further reveal that, unlike canonical PPR factors that act on a single or a few closely related transcripts, PPR9 is essential for the splicing of several mitochondrial introns, including *nad2* intron 3 and *nad7* introns 1 and 2. These defects lead to impaired biogenesis of the respiratory CI enzyme and disrupted OXPHOS activities in the mutants. Together, these findings demonstrate that PPR9 plays a key role in RNA maturation in Arabidopsis mitochondria, enabling proper CI biogenesis and cellular energy metabolism. This work highlights the broader importance of nuclear-encoded RNA-processing enzymes in coordinating mitochondrial function, plant physiology and early developmental processes in plants.

Key words

Pentatricopeptide (PPR) proteins; mt-RNA metabolism; splicing; group II introns; mitochondria; *Arabidopsis thaliana*.

Significance statement

Our study identifies PPR9 as a key mitochondrial RNA-processing factor required for the splicing of multiple group II introns that reside within genes encoding subunits essential for respiratory complex I biogenesis in Arabidopsis. By linking nuclear control of RNA maturation to mitochondrial function and plant development, this work emphasizes a critical layer of

coordination between organellar gene expression, energy metabolism, and developmental regulation in plants.

Introduction

Mitochondria are essential organelles that function as key sites of energy production, and as hubs for diverse and essential metabolic and signaling pathways in eukaryotic cells (Braun 2020, Millar *et al.* 2011, Møller *et al.* 2021). Mitochondria in plants also contribute to key developmental processes, such as stress responses and developmental regulation. As remnants of an ancestral α-proteobacterial endosymbiont, most mitochondria retain their own genome (mtDNA, mitogenome), with intrinsic transcriptional and translational apparatuses (Gualberto and Newton 2017). However, the large majority of mitochondrial proteins, and some tRNAs, are encoded by nuclear loci and imported into the organelles. A physical separation of the two remote genetic systems (i.e., nucleus and mtDNAs) requires a coordinated expression and assembly of the nuclear- and mitochondria-encoded proteins of the oxidative phosphorylation (OXPHOS) system. These complex regulated molecular processes are pivotal to ensure respiration, and hence cellular homeostasis, which are vital to support normal plant growth and development.

Although seem to share a common ancestor, mitochondria have diverse considerably in different taxa. Plant and fungi mitogenomes differ markedly from their animal counterparts in both size and structural complexity. While animal mtDNAs are more compact (typically around 17 kb in size), the sequenced mtDNAs from various angiosperms can range from ~70 kb to over 10 Mb, and often exhibit multipartite and recombinationally active structures (Gualberto and Newton 2017). This genetic complexity is further evident in mitochondrial gene expression, where plant organellar pre-RNAs undergo extensive post-transcriptional processing, including trimming, editing and splicing, to produce functional non-coding RNAs (i.e., rRNAs, or tRNAs) and mRNAs that translate into the correct organellar proteins (Hammani and Giege 2014, Small *et al.* 2023, Zmudjak and Ostersetzer-Biran 2018).

A prominent feature of plant mitogenomes is the high abundance of group II-related intron sequences that disrupt (mostly) protein-coding genes, particularly those encoding subunits of the NADH dehydrogenase enzyme (i.e., complex I, CI), as well as genes encoding cytochrome c oxidase (complex IV, CIV) subunits, cytochrome c maturation (CCM) factors, ribosomal protein biogenesis and may reside in other genes as well (Bonen 2008, Brown *et al.* 2014, Schmitz-

Linneweber *et al.* 2015, Zmudjak and Ostersetzer-Biran 2018). Introns of this group are ancient catalytic RNAs that are evolutionarily related to spliceosomal introns, non-LTR retroelements, and telomerases (Lambowitz and Belfort 2015, Zhao and Pyle 2017b, Zimmerly and Semper 2015). The group II RNAs fold into a conserved structure comprising six domains (D1–D6) that facilitates the two sequential trans-esterification reactions necessary for splicing (Zimmerly and Semper 2015). Canonical group II introns can self-splice under high salt and temperature conditions *in vitro*, but *in vivo* excision relies on protein cofactors, such as the cognate intron-encoded maturases (MATs), which likely assist or stabilize the intron structure to enable efficient RNA catalysis (Mizrahi *et al.* 2022, Zhao and Pyle 2017a). Throughout evolution, the plant mitochondrial introns have diverged extensively in sequence and have often lost their own intron-encoded maturases (Mizrahi *et al.* 2022). In some cases, the introns have further fragmented into independently transcribed gene segments that must assemble *in trans* to facilitate exon splicing (Bonen 2008). These structural and sequence alterations have likely coincided with the recruitment of numerous nuclear-encoded RNA-binding cofactors (Hammani and Giege 2014, Mizrahi and Ostersetzer-Biran 2024, Mizrahi *et al.* 2022, Small *et al.* 2023, Zmudjak and Ostersetzer-Biran 2018) that facilitate intron folding (or splicing), thus enhancing the level of regulation of organellar gene expression (Brown *et al.* 2014). Organellar group II intron splicing relies on a diverse set of nuclear-encoded protein cofactors, including factors evolutionarily related to maturases (nMATs), various RNA helicases, mTERFs, and PORR-domain proteins, as well as members of the greatly expanded pentatricopeptide repeat (PPR) protein family in plants that are in the focus of this study.

High-throughput genome sequencing has revealed that PPR proteins constitute one of the largest protein families in land plants (Small and Peeters 2000), with approximately 450 members in *Arabidopsis thaliana*. These abundant factors are characterized by tandem repeats of a degenerate 35-amino acid motif that assembles into a helix-turn-helix structure, enabling the modular and sequence-specific recognition of single-stranded RNA, with each PPR motif binding to a specific ribonucleotide (Barkan and Small 2014, Gully *et al.* 2015b, Shen *et al.* 2015). Most PPR proteins are targeted to mitochondria or chloroplasts, where they regulate diverse aspects of organellar RNA metabolism, including RNA trimming, transcript stabilization, RNA base editing, the splicing of group II introns (Gutmann *et al.* 2020, Hammani and Giege 2014, Lenz *et al.* 2018, Schallenberg-Rüdinger *et al.* 2013, Small *et al.* 2023, Zmudjak and Ostersetzer-Biran 2018), and

also appear to participate in the regulation of translation, as well (Grüttner *et al.* 2022, Rugen *et al.* 2024, Waltz *et al.* 2019).

Substantial progress has been made in decoding the RNA-recognition code of PPR proteins and in assigning roles for these factors in the processing of their defined RNA targets, but the precise molecular mechanism by which individual PPR factors assist in intron folding and splicing remain much less well understood. Here, we characterize PPR9 (encoded by the *AT1G03560* gene-locus), a P-class PPR protein that is essential for early embryo development in *A. thaliana*. Genetic, molecular and biochemical analyses reveal that At.PPR9 functions as a splicing factor. Specifically, loss of PPR9 impairs the excision of *nad2* intron 3 and *nad7* introns 1 and 2, leading to defects in respiratory CI biogenesis, and consequently to severe developmental and physiological defects. These findings expand our understanding of the roles played by nuclear-encoded RNA binding cofactors in the complex post-transcriptional regulation of mitochondria gene expression, and highlight the importance of PPR9 in organellar RNA maturation, maintaining mitochondrial OXPHOS function and overall plant viability.

Results

PPR9 (*AT1G03560*) gene encodes a P-type PPR protein with a broad range of putative RNA-binding sites

To gain deeper insights into the mechanisms of mt-RNA processing steps in plants, we screened a collection of publicly available *A. thaliana* T-DNA insertional mutants (i.e., The Arabidopsis Information Resource, TAIR, database) that reside in genes that encode putative mitochondria-targeted P-type PPR proteins. Among these, we noticed that heterozygous plants carrying an insertion in the *AT1G03560* gene-locus (UniProt Q9LR67, or PPR9_ARATH) failed to yield viable homozygous offspring. The deduced product of *PPR9* locus (Fig. 1a, Supplementary Fig. S1a) harbors a 660-amino acid protein with a predicted topology of NH_2-151-(P)-P-P-P-P-P-P-P-P-P-P-P-P-P-P-19-COOH (Cheng *et al.* 2016, Yan *et al.* 2019), where 'P' denotes 13 canonical P-type (helix-turn-helix) PPR domains, the motif shown in quotes represents a degenerated PPR domain, while numbers correspond to amino acid residues not assigned to any defined motif (Figs. 1a, 1b). Subcellular localization predictions from TargetP (Emanuelsson *et al.* 2000), UniProt (Wu *et al.* 2006) and SUBA4 (Hooper *et al.* 2017), predict the presence of a 53-amino acid mitochondrial targeting signal at the N-terminus of the PPR9 protein (Fig. 1a). *In silico* 3D

modeling of Arabidopsis PPR9 with AlphaFold (Jumper *et al.* 2021) further indicated a canonical superhelical solenoid fold (Fig. S1), containing an internal basic groove within the molecule that is consistent with RNA-binding regions described for PPR proteins (Gully *et al.* 2015a, Gully *et al.* 2015b, Shen *et al.* 2016).

PPR proteins typically act as sequence-specific RNA-binding factors (Barkan and Small 2014, Gully *et al.* 2015b, Shen *et al.* 2015, Small *et al.* 2023, Small *et al.* 2020). Their RNA recognition is based on a combinatorial amino acid code defined largely by residues at positions 5 and 35 (or last in non-canonical PPR domains) of each PPR motif, which together guide the nucleotide binding site of individual PPR domains (Barkan *et al.* 2012, Cheng *et al.* 2016, Takenaka *et al.* 2013). In some cases, certain PPR proteins exhibit predicted binding sites that accurately reflect their specific RNA targets, predictions that were later validated through genetic analyses; see e.g., (Best *et al.* 2023). In other cases, however, the predicted RNA-binding sites are less defined, or insufficient to accurately identify the true target sequence *in silico*. When the 'PPR code' was applied to the 13 canonical motifs of PPR9, it yielded a very broad range of potential target sites (Table S1) within the updated mitogenome sequence (BK010421) of Arabidopsis (Sloan *et al.* 2018). In total, 203 putative PPR9 recognition sites were identified. Excluding non-coding/intergenic regions of the Arabidopsis mitogenome (Best *et al.* 2020b, Sloan *et al.* 2018), the remaining sites were distributed across multiple gene regions: 19 sites were located within 5′ and 3′ untranslated (UTR) regions, 51 sites within exonic sequences, and 54 sites within intronic regions (Table S1). The extensive set of predicted targets for PPR9 likely indicates that the current binding code is insufficient to precisely determine its RNA target *in silico*. Alternatively, a more 'promiscuous' RNA recognition code may enable interactions with multiple RNA targets *in vivo*. This ambiguity underscores the need for complementary genetic and biochemical approaches to elucidate the precise molecular function of PPR9 in mt-RNA metabolism, by establishing its intracellular location(s), the RNA targets and roles in gene expression, *in vivo*. Figure 1b shows the predicted binding code for three mitochondrial introns (i.e., *nad2* intron 3 and *nad7* introns 1 and 2) that were validated as PPR9 RNA substrates through our genetic analyses.

PPR9 **encodes a lowly-expressed mitochondria-localized PPR protein**

Expression analysis of PPR9 was carried out using publicly available microarray and high-throughput sequencing datasets (Huala *et al.* 2001, Luna-García *et al.* 2023). These databases

indicate that PPR9 displays differential expression across developmental stages, with elevated transcript levels in embryonic tissues, young developing leaves, apical root regions, flowers, and the shoot apex (Fig. S2). Here, we further analyzed the intracellular location of PPR9 protein, *in vivo*. For this purpose, we created an in-frame fusion protein containing the first 82 amino acids of PPR9 with eGFP (PPR9-GFP), and expressed it in protoplasts prepared from *Physcomitrium patens*, a model moss that provides stable protoplasts suitable for land plant GFP localization analyses (Thévenin *et al.* 2012, Thévenin *et al.* 2016, Wang *et al.* 2017). Confocal microscopy analyses showed that the PPR9-GFP fluorescence signals appear as globular-shaped particles that co-localized with MitoTracker, a mitochondrion specific fluorescent probe (Fig. 2). These results support *in silico* predictions and MS/MS data (Fuchs *et al.* 2020) that PPR9 is targeted to the mitochondria, where it is postulated to function in post-transcriptional regulation of organellar gene expression or RNA metabolism (Hammani and Giege 2014, Small *et al.* 2023, Zmudjak and Ostersetzer-Biran 2018).

PPR9 is indispensable for (early) embryogenesis in *Arabidopsis thaliana*

Analysis of the SIGnAL (Salk Institute Genomic Analysis Laboratory) database identified a single T-DNA line (SALK_004994) within the coding sequence of PPR9, inserted 536 nucleotides downstream of the translational initiation (AUG) start site (Fig. 1a). Genetic screening revealed that under optimal growth conditions (i.e., 22°C, long-day conditions with 100~150 μmol m^{-2} s^{-1} light intensity and 50% RH), no homozygous plants could be obtained from the progeny of heterozygous *ppr9* line (Fig. 3a), indicating that the function of *AT1G03560* gene is essential during embryogenesis. Under the optimal growth conditions, heterozygous *ppr9* plants exhibited no visible abnormalities, suggesting that the complete loss of PPR9 functions result in embryonic lethality. We also examined the developmental phenotypes of embryos in immature seeds (10 days after pollination) from heterozygous and wild type plants. Siliques from heterozygous *ppr9* plants contained approximately one-quarter of white seeds (Fig. 3b), which later degenerated into shrunken and darkened seeds upon maturation (Fig. 3a). Microscopic (Nomarski, DIC) analysis further revealed that the green seeds contained fully developed embryos, whereas white seeds collected from the same siliques harbored embryos arrested at the late torpedo to walking-stick stages of development (Fig. 3b). These phenotypes are also associated with various Arabidopsis

mutants defective in mt-RNA metabolism (Colas des Francs-Small and Small 2014, Ostersetzer-Biran 2016).

PPR9 functions are required for proper mitochondrial transcript processing in *A. thaliana*

Embryo rescue techniques have been successfully applied to recover certain Arabidopsis mutants exhibiting germination-defective phenotypes (Franzmann *et al.* 1989). Similar approaches have been used and modified for several mutants impaired in mitochondrial biogenesis and function, including *cod1* (Dahan *et al.* 2014), *ndufv1* (Kuhn *et al.* 2015) *cal1/cal2* (Cordoba *et al.* 2016, Fromm *et al.* 2016), *nmat3* (Shevtsov-Tal *et al.* 2021) and *msp1* (Best *et al.* 2023). Following our lab strategy (Best *et al.* 2023, Shevtsov-Tal *et al.* 2021), white seeds collected from green-mature siliques of heterozygous *ppr9* plants (10-12 days post-anthesis, DPA) were plated on (½) MS-agar plates supplemented with 3% sucrose and a vitamin mix, and transferred to a controlled growth chamber (Fig. 3c). Under in vitro conditions, between 20 to 30% of the white seeds germinated after about 1~3 months (Fig. 3c-i). To increase biomass yield for downstream analyses (e.g., BN-PAGE), seedlings at the L6 stage (Boyes *et al.* 2001) were transferred to liquid (½) MS medium and cultured under the growth conditions (specified in the 'Plant material and growth conditions' section), with gentle agitation (50-100 rpm). Most of these seedlings died within two to four weeks after germination, or following their transfer to a liquid MS medium (Fig. 3c-i, Fig. S3), and only a few (approximately 20% of those germinated) were able to survive and be maintained (Fig. 3c-ii, Fig. S3). PCR-based genotyping confirmed that while the green seeds from heterozygous *ppr9* plants were either wild type or heterozygous for SALK_004994 (Figs. 3c-ii, 3c-iii), while plantlets regenerated from white seeds (Figs. 3c-ii, 3c-iv) were homozygous for the *PPR9* mutant allele. As previously noted for various embryo-defective (*emb*) mutants (Boyes *et al.* 2001), particularly those with defects in mitochondrial biogenesis (Best *et al.* 2023, Colas des Francs-Small and Small 2014, Dahan *et al.* 2014, Kuhn *et al.* 2015, Shevtsov-Tal *et al.* 2021), a growth retardation and phenotypic variability was also observed among the rescued *ppr9* plantlets (Figs. 3c-ii, 3c-iv, Fig. S3). No homozygous *ppr9* plantlets could be successfully established in soil, and none of the rescued plants were able to complete their life cycle or produce viable seeds.

The steady-state levels of mitochondrial coding sequences in *ppr9* mutant line were analyzed by RT-qPCR and compared with wild type (Col-0) plants. This analysis revealed a notable reduction (~250-fold) in the accumulation of *nad2* transcripts corresponding to excised exons '3'

and ‘4’ (*i.e.*, *nad2* ex3-4) in *ppr9* mutant seedlings (Fig. 4a). We also noticed reduced levels of transcripts corresponding to spliced *nad7* exons ‘1’ and ‘2’ (*nad7* ex1-2, about 8-fold lower) and spliced *nad7* exons ‘2’ and ‘3’ (*nad7* ex2-3, about 20-fold lower) in the *ppr9* plantlets. Importantly, the RNA profiles of wild type plants (Col-0) correspond to plantlets derived from immature wild type embryos propagated in vitro under the same conditions as those of the rescued homozygous *ppr9* plants, showed no significant alterations in mitochondrial transcript accumulation, including *nad2* and *nad7* transcripts. Likewise, the steady-state levels of *nad2* and *nad7* transcripts in the functionally complemented (*ppr9/PPR9*) line were comparable to those seen in the wild type plants (Fig. 4a). Taken together, these data indicate that the defects in the processing or maturation of the *nad2* and *nad7* transcripts are attributable to the loss of PPR9 function, and are not a consequence of the embryo-rescue procedure.

PPR9 is required for efficient splicing of *nad2* intron 3 and *nad7* introns 1 and 2

Based on the reduced steady-state levels seen for *nad2* ex3-4, *nad7* ex1-2 and ex2-3 transcripts in *ppr9* mutants (Fig. 4), we assumed that these changes could correspond to defects in the splicing of *nad2* intron 3 and *nad7* introns 1 and 2, respectively. To test this assumption, we quantified the splicing efficiencies of the 23 mitochondrial introns in germinated embryos of wild type plants, the *ppr9* mutant line and functionally complemented *ppr9/PPR9* plants. Splicing efficiency was first evaluated by RT-qPCR, by calculating the ratios of pre-RNAs to their corresponding excised mRNAs in mutant lines versus wild type plants. The RT-qPCR results showed an impairment in the processing of *nad2* intron 3, with an approximately 1,000-fold reduction in splicing in the mutant relative to the wild type plants (Fig. 5a). Similarly, the splicing efficiencies of *nad7* introns 1 and 2 were also affected, showing about 30- and 60-fold reductions, respectively (Fig. 5a). The splicing efficiencies of other mitochondrial introns were comparable to those of the wild type or only mildly affected (not statistically significant) in the homozygous mutant (Fig. 5a). The processing of these transcripts in the functional complemented *ppr9* line (*ppr9/PPR9*) were equivalent to those of the germinated wild type embryos (used as a reference in the RT-qPCR reactions), underscoring the essential role of PPR9 in the processing of these three mitochondrial group II-type RNA introns (Fig. 5b).

These data were also analyzed by RNase protection assays, which revealed defects in the processing of *nad2* intron 3 and *nad7* introns 1 and 2 (Fig. S4) in the *ppr9* mutant. In contrast, the

processing of intron-containing *cox2* and *rpl2* transcripts, as well as the accumulation of the intronlerss *nad6* mRNA transcript (i.e., doesn't harbor an intron in *A. thaliana* mitochondria), were unaffected. We observed an accumulation of pre-RNA corresponding to the *trans*-spliced *nad2* intron 2 in the *ppr9* mutant (Fig. S4). Since the accumulation of *nad2* exon 2-3 transcripts was only slightly affected in the mutant (Figs. 4, 5, and S4), we assume that an accumulation of precursor *nad2* intron 2 RNAs may results from the sequential nature of *nad2* splicing, where impaired processing of intron 3 (the RNA substrate of PPR9) likely affect the processing of a related product, the precursor *nad2* intron 2 transcripts. Accordingly, across multiple introns within a single gene (e.g., *nad1*, *nad2*, *nad4*, *nad5*, and *nad7*), there may be no single universal order of processing, and the RNA processing steps are interdependent. For example, the splicing or availability of one exon-intron segment seem to influence the substrate for the subsequent step, particularly in *trans*-spliced introns such as *nad1*, *nad2*, and *nad5*. Examples include cases where the loss of a single splicing factor, e.g., OTP43 (Falcon de Longevialle *et al.* 2007) or MSP1 (Best *et al.* 2023) that function in *nad1* intron 1 processing, affect 'downstream' RNA processing steps. Also, coupling between RNA editing within specific transcripts and the splicing of adjacent introns has also been demonstrated for particular RNA maturation factors (Castandet *et al.* 2010, Farre *et al.* 2012).

Protein profiling of respiratory complexes and organellar proteins by BN-PAGE, SDS-PAGE and immunoblotting

The mitochondrial respiratory system consists of five major protein complexes: CI (~1,000 kDa), CII (~160 kDa), a dimeric complex III ($CIII_2$, ~500 kDa), CIV (200–220 kDa), and the ATP synthase (CV, ~660 kDa) enzyme. In addition to the canonical respiratory complexes, plant mitochondria also harbor enzymes of the alternative electron transport pathway, including rotenone-insensitive NADH dehydrogenases (NDs) and alternative oxidases (AOXs) (Braun 2020, Millar *et al.* 2011, Møller *et al.* 2021). The incorporation of NAD2 and NAD7 subunits is essential for the assembly of a functional holo-complex I in plants (Braun 2020, Ligas *et al.* 2019, Meyer *et al.* 2019, Ostersetzer-Biran 2016). The reductions we observed in the maturation of *nad2* and *nad7* pre-RNA transcripts (Figs. 4, 5) suggest that these subunits are either absent or present only at low levels in *ppr9* mutants. Consistent with this, BN-PAGE analysis of Arabidopsis mitochondrial respiratory complexes revealed to altered CI biogenesis in homozygous *ppr9* mutants (Fig. 6).

These were apparent by immunoblotting with antibodies against the carbonic anhydrase subunit CA2 (membranous domain) and the Nad9 protein (soluble arm), which indicated that holo-CI was undetectable in homozygous *ppr9* mutants as well as to the accumulation of various CI assembly intermediates (in the CA2 blots) with lower molecular masses in *ppr9* plants. Similar CI-assembly intermediates have been reported in various Arabidopsis mutants defective in CI biogenesis (Braun *et al.* 2014, Kuhn *et al.* 2015, Ligas *et al.* 2019, Meyer *et al.* 2019, Ostersetzer-Biran 2016). Consistent with this assumption, the lower-mass CI-associated particles were absent from the NAD9 blot (Fig. 6). We also compared the relative accumulation of mitochondrial complexes in germinated seedlings of wild type (Col-0) and the functionally complemented line *ppr9/PPR9* plants, by BN-PAGE followed by immunoblotting with antibodies against several mitochondrial proteins, as indicated in Figure 6. These analyses demonstrated that the levels of CI (as indicated by immunoblots to CA2 and Nad9 subunits), CIII (Rieske iron–sulfur protein, RISP), CIV (Cox2 subunit), and CV (AtpA and AtpB subunits) in *ppr9/PPR9* seedlings were comparable to those observed in the wild type plants. Table S2a indicates the relative accumulation of organellar respiratory complexes in wild type and mutant plants.

The steady-state levels of the mitochondrial gamma carbonic anhydrase-like 2 (CA2, ~30 kDa), was found lower (about 50%, Table S2b) to those of the germinated wild type embryos (Col-0 heart), and the functionally complemented *ppr9* line *(ppr9/PPR9*) (Fig. 7). The levels of the CI NAD9 subunit of the soluble arm (~23 kDa) was notably reduced (about 6% of that seen in the wild type plants) (Fig. 7, Table S2b). The signals of cytochrome b-c1 complex subunit Rieske-1 (RISP, ~29 kDa) of complex III, cytochrome c oxidase subunit 2 (COX2, ~30 kDa) and the Voltage-dependent anion-selective channel protein 1 (VDAC1, ~29 kDa), were all found to be somewhat higher than those of the germinated wild type embryos collected from the same siliques (Fig. 7, Table S2b). The steady-state levels of alternative oxidase 1a protein (AOX1a, ~33 kDa) were notably increased (about 250-fold) in *ppr9* mutant (Fig. 7, Table S2b). Using equivalent amounts of fresh weight tissue, the respiratory complexes were found to be somewhat lower in the functionally complemented *ppr9/PPR9* plants than in the wild type plants (Fig. 7, Table S2b). These patterns may relate to the presence of a single copy of the *PPR9*, which could result in altered expression across tissues and lead to altered mitochondrial biogenesis, or may not fully reproduce the native expression pattern of the wild type plants.

Discussion

PPR9 encodes a mitochondrial P-type PPR protein essential for early embryogenesis

Mitochondria are central hubs of eukaryotic energy metabolism and are indispensable for angiosperm physiology. During the evolution of land plants, the mitogenomes (mtDNAs) seem to have acquired remarkable structural plasticity, with extensive variation in genome size, architecture and expression patterns (especially at the RNA level) among species (Best *et al.* 2020a, Broz *et al.* 2025, Gualberto and Newton 2017, Knoop 2012). Expression of mitochondrial genes in plants requires a multitude of post-transcriptional processing steps, including RNA cleavage, exonucleolytic trimming, RNA editing, and, relevantly for this study, the splicing of numerous group II introns embedded within the coding regions of many essential mitochondrial proteins (Colas des Francs-Small and Small 2014, Hammani and Giege 2014, Small *et al.* 2023, Zmudjak and Ostersetzer-Biran 2018). These processing steps seem to serve as major regulatory checkpoints and rely on a diverse set of RNA-binding cofactors. Here, we focused on Arabidopsis PPR9, a P-type PPR protein factor, encoded by the *AT1G03560* gene-locus. *In silico* analyses indicate that PPR9 encodes a lowly expressed, mitochondria-targeted P-type PPR protein containing 13 or 14 tandem PPR motifs (Figs. 1, S1). Global MS/MS data (Fuchs *et al.* 2020) and our GFP localization analysis further support the *in vivo* targeting of PPR9 to mitochondria (Fig. 2). Using an embryo-rescue approach (Figs. 3, S3), we established a homozygous *ppr9* (SALK_004994) mutant line, which allowed us to demonstrate that PPR9 is required for the mitochondrial RNA metabolism and genes expression (Figs. 4, 5, S4). RNase-protection and RT-qPCR assays indicate a role for PPR9 as a key regulator of *nad2* and *nad7* transcripts maturation and hence in respiratory CI biogenesis (Figs. 6, 7) and normal embryo development in Arabidopsis plants (Figs. 3, S3).

PPR9 promotes the splicing of several group II-type introns within *nad2* and *nad7* genes

The majority of plant mitochondrial introns belong to the group II intron family (Bonen 2008, Brown *et al.* 2014, Lambowitz and Belfort 2015, Schmitz-Linneweber *et al.* 2015, Zimmerly and Semper 2015). Unlike canonical autocatalytic group II introns, the splicing of plant mitochondrial introns relies on a large set of protein cofactors. These mainly include nuclear-encoded RNA-binding factors, some of which are closely related to key splicing factors such as maturases (Lambowitz and Belfort 2015, Lambowitz and Zimmerly 2011, Mizrahi *et al.* 2022, Zhao and Pyle

2017a) or RNA helicases (Mizrahi and Ostersetzer-Biran 2024, Russell *et al.* 2013). Others belong to a broad array of RNA-binding proteins that were probably recruited during evolution to facilitate the splicing of the highly degenerated mitochondrial introns in plants (Bonen 2008, Brown *et al.* 2014, Schmitz-Linneweber *et al.* 2015). Among these, PPR proteins constitute a particularly large family in angiosperms, comprising ~450 members in Arabidopsis (Barkan and Small 2014, O'Toole *et al.* 2008, Schmitz-Linneweber and Small 2008, Small and Peeters 2000). These proteins are postulated to bind single-stranded RNA in a modular and sequence-specific manner, and have been shown to play key roles in organellar RNA stabilization, editing, cleavage, intron removal (Small *et al.* 2023, Small *et al.* 2020, Takenaka *et al.* 2019, Zmudjak and Ostersetzer-Biran 2018), as well as in mitoribosome biogenesis and translation (Kwasniak-Owczarek *et al.* 2019, Rugen *et al.* 2019, Waltz *et al.* 2019).

Genetic characterization of *ppr9* mutants showed that homozygous plants could only be recovered and established under *in vitro* conditions (Figs. 3, S3), through embryo-rescue techniques. Analysis of the RNA profiles revealed a notable reduction in the steady-state levels of processed transcripts corresponding to *nad2* exons 3-4 and *nad7* exons 1-2 and exons 2-3, in *ppr9* mutants (Figs. 4, S4). Splicing assays further indicated that the removal of intron 3 of *nad2* and introns 1 and 2 of *nad7* was affected in the mutant (Figs. 5, S4).

Some PPR proteins exhibit binding predictions that designate a single or a few closely related sites that can also be biologically validated as RNA targets. Yet, PPR9 displays a more degenerate recognition pattern. Computational predictions using the PPR code (Cheng *et al.* 2016, Yan *et al.* 2019) identified over 200 potential binding sites for PPR9 (excluding intergenic regions), distributed across exonic, intronic and UTR regions. This may suggest either a limitation of the current PPR code in accurately predicting a specific RNA target(s), or maybe relate to a promiscuous binding mode enabling interactions with multiple RNA substrates, as noted for PPR9 protein *in vivo*. Experimental validation, including *in vitro* RNA-binding assays, will be required to determine whether PPR9 binds its genetically identified RNA substrates directly, as typically shown for canonical PPR proteins (Rovira and Smith 2019, Small *et al.* 2023, Zmudjak and Ostersetzer-Biran 2018). However, PPR9 may also act in splicing by recruiting other splicing cofactors.

Our findings establish that PPR9 functions in the maturation of *nad2* and *nad7* transcripts, with 'downstream consequences' for CI assembly and embryonic viability. Notably, the three

genetically validated targets of PPR9 (i.e., *nad2* intron 3, and *nad7* introns 1 and 2) are also identified among the predicted RNA targets for this protein in the *in silico* assays (Table S1).

PPR9, complex I assembly, and embryo development

The mitochondrial electron transport chain (ETC) comprises four main complexes (CI–CIV) that generate a proton gradient across the inner membrane, driving ATP biosynthesis by the ATP synthase (CV) enzyme (Braun 2020, Millar *et al.* 2011, Møller *et al.* 2021). In addition to the canonical respiratory complexes, plants (and other organisms) possess alternative oxidases (AOXs) and rotenone-insensitive NAD(P)H dehydrogenases (NDs) that bypass the classical ETC system (Braun 2020, Møller *et al.* 2021). CI, the largest respiratory complex (~1,000 kDa), is composed of about 50 subunits, derived from expression of both mitochondrial (*nad1-nad7*, nad9) and nuclear genomes loci (Klusch *et al.* 2023, Klusch *et al.* 2021, Maldonado *et al.* 2020, Soufari *et al.* 2020). These subunits assemble into the 'membrane-embedded' and 'matrix-associated' subdomains, which together form the functional holoenzyme, and further assemble into respiratory chain 'supercomplexes'(Braun 2020, Formosa *et al.* 2018, Guerrero-Castillo *et al.* 2017, Ligas *et al.* 2019, Meyer *et al.* 2019, Ostersetzer-Biran 2016, Senkler *et al.* 2017, Subrahmanian *et al.* 2016). The NAD2 and NAD7 subunits play pivotal roles in assembling the membrane arm and matrix arm, respectively (Ligas *et al.* 2019). Accordingly, we found that *ppr9* mutants, which are defective in *nad2* and *nad7* splicing, exhibited a dramatic reduction in CI levels, as revealed by BN-PAGE (Fig. 6). Immunoblotting with anti-CA2 antibodies further identified distinct CI intermediates, including an ~85 kDa particle (Fig. 6, CA2 panel), previously described in *abo5* (Ligas *et al.* 2019, Liu *et al.* 2010) or *misf2* (Nguyen *et al.* 2022) mutants that are deficient in *nad2* expression. Higher molecular-mass particles observed in *ppr9* likely represent non-canonical assembly intermediates lacking NAD2.

We also link CI biogenesis defects to altered embryogenesis. The degree of CI deficiency has previously been correlated with phenotypic severity in Arabidopsis mutants (Colas des Francs-Small and Small 2014, Kuhn *et al.* 2015, Ostersetzer-Biran 2016). Mutants with a strong decrease in holo-CI often produce embryos arrested at early developmental stages, likely due to both altered cellular functions and insufficient nutrient reserves in the seed. Similarly, mutants defective in fatty acid β-oxidation display comparable phenotypes of altered embryo development (Pinfield-Wells *et al.* 2005). Likewise, homozygous *ppr9* mutants exhibit early embryonic arrest, with white

immature seeds failing to germinate under 'standard' conditions (Figs. 3, S3). In some cases, germination could be rescued under *in vitro* conditions using enriched growth media. The precise molecular mechanism underlying this rescue remains unclear. It is possible that the additional minerals, sugars or vitamins support essential metabolic functions or compensate for metabolic constrains in mutant seeds. Alternatively, prematurely harvested seeds with a softer seed coat (Huss and Gierlinger 2021) may facilitate the emergence of the embryo's radicle and hypocotyl, by increasing permeability and reducing mechanical resistance. The few germinated *ppr9* seedlings displayed stunted growth and other phenotypes (Figs. 3c, S3) characteristic of CI-deficient plants (Colas des Francs-Small and Small 2014, Kuhn *et al.* 2015, Ostersetzer-Biran 2016). While external sugars and vitamins allowed limited vegetative development, the mutants could not complete their life cycle or produce viable seeds, underscoring the essentiality of PPR9 and mt-RNA maturation steps for mitochondria biogenesis, respiration, organellar-related metabolism and plant physiology.

Materials and methods

Plant material and growth conditions

The experiments involved *Arabidopsis thaliana* (Col-0) plants. Seeds of the wild type and the *ppr9* mutants (SALK_004994) were obtained from the Arabidopsis Biological Resource Center (ABRC, Ohio State University, USA). For germination on half-strength (½) Murashige and Skoog (MS)-agar medium (M0221, Duchefa Biochemie, Haarlem, Netherland) wild type and mutant seeds were sterilized with Cl_2 gas and sown on MS-agar plates supplemented with 1% (w/v) sucrose or rescued using the method detailed below. After a 5-day stratification period at 4 °C, the plates were transferred to a growth chamber (Percival Scientific, Perry, IA, USA) set to 22°C with long-day conditions (16 h light/8 h dark), RH 50%, with a light intensity of 100~150 µE m^{-2} s^{-1}. The identity and integrity of each line were confirmed by PCR genotyping using gene-specific and T-DNA-specific primers (Table S3). Seeds from confirmed lines were sterilized, germinated on MS-agar medium containing 1% sucrose, and analyzed for their associated genetic and biochemical phenotypes. For larger-scale biomass production (e.g., for BN-PAGE analysis), seedlings from the MS-agar plates were transferred and grown in liquid MS medium supplemented with sucrose and vitamins (see below, 'Embryo-rescue and establishment of a homozygous *ppr9* mutant line'), with moderate shaking (50–100 rpm) (Shevtsov-Tal *et al.* 2021).

Embryo-rescue and establishment of a homozygous *ppr9* mutant line

Embryo rescue of the *ppr9* mutant line was performed essentially as described previously (Best *et al.* 2023, Shevtsov-Tal *et al.* 2021). In brief, mature green siliques from heterozygous *ppr9* plants were surface-sterilized and then rinsed thoroughly with sterile DDW. Green (wild type or heterozygous) and white (homozygous *ppr9*) seeds isolated from the sterilized siliques were sown on MS-agar plates supplemented with 3% (w/v) sucrose and a vitamin mix (i.e., 100 µg myoinositol, 1.0 µg thiamine, 1.0 µg pyridoxine, 1.0 µg nicotinic acid per liter of media). To obtain larger quantities of plant material, required for BN-PAGE analyses, seedlings at the 6 leaves (L6) stage (Boyes *et al.* 2001) were transferred to a liquid MS medium containing 1-3% sucrose and the same vitamin mix and grown under the conditions described previously, with gentle agitation (50-100 RPM), as we performed previously (Best *et al.* 2023, Shevtsov-Tal *et al.* 2021).

Imaging-based analysis of Arabidopsis plant tissues

For morphological analyses, plant tissues were examined using a stereoscopic (dissecting) microscope or a light microscope at the Bio-Imaging Unit, Institute of Life Sciences, The Hebrew University of Jerusalem.

Protoplasts preparation from *P. patens* and GFP localization assays

Physcomitrium patens protoplasts were prepared and transformed generally as previously described (Charlot *et al.* 2022), with minor modifications. In brief, protoplasts were obtained from harvested tissue of a 1-month-old liquid culture (protonemata enriched) and treated with 4% (w/v) Driselase in 0.5 M mannitol. The resulting suspension was filtered through a 45 µm sieve. A DNA product encoding the first 82 amino acids of the intronless *PPR9* gene, fused in-frame to eGFP, was cloned into the binary pCAMBIA-1302 vector (CAMBIA, Canberra, Australia; https://www.cambia.org; GenBank AF234298.1) under the control of CaMV 35S promoter and a NOS terminator. The pCAMBIA-1302-N-PPR9-eGFP construct was then introduced into the *P. patens* protoplasts by PEG 4000 transformation method (Schaefer *et al.* 1991). For transformation, protoplasts were pelleted by centrifugation (10 min, 50 ×g, at 25 °C), and approximately 1.2×10^5 cells were incubated with 30~50 µg of plasmid DNA suspended in 0.1 M $Ca(NO_3)_2$ within a 25% (w/v) PEG 4000 solution. Transformed cells were imaged 72 h post-transformation using an

Olympus FV3000 confocal microscope, and the resulting images were visualized and processed with the Fiji open-source software (Schindelin *et al.* 2012).

Mitochondrial transcript analysis in wild type and mutant plants

Total RNA was extracted from approximately 50 mg of plant tissue using RNAzol® RT (R4533, Sigma-Aldrich, Rehovot, Israel) reagent. The isolated RNA was subsequently treated with RNase-free DNase I to remove DNA prior for its use in RT-qPCR analysis. In brief, cDNA was synthesized from 1-3 µg of total RNA using SuperScript III First-Strand Synthesis System for RT-PCR (Cat. no. 18080-051, Invitrogen, Rhenium Modi'in, Israel). RNA (11 µl of total RNA in nuclease-free water) was mixed with 1 µl dNTP mix (2.5 mM each nucleotide) and 1 µl random hexamers (1 µg/ml), incubated at 65 °C for 5 min, and immediately chilled on ice for 5 min. A reaction mix containing 4 µl 5× 'First Strand' buffer, 1 µl DTT, 1 µl RNasin RNase inhibitor, and 1 µl SuperScript III, for each cDNA synthesis reaction, was prepared on ice, and added to each RNA sample. Samples were then incubated at 25°C for 5 min for primer annealing, followed by 60 min at 50°C for cDNA synthesis, and 15 min at 70°C to inactivate the enzyme. Gene-specific oligonucleotides were designed to amplify both mRNA and pre-mRNA transcripts (Table S4) in qPCR. For normalization, *Arabidopsis thaliana* reference genes, *GAPDH* (*AT1G13440*), *ACTIN2* (*AT3G1878*), and *18S rRNA* (*AT3G41768*), were used as internal calibrators. RNase-protection assays (Cohen *et al.* 2014, Keren *et al.* 2009, Keren *et al.* 2012, Ostersetzer *et al.* 2005) were performed with *in vitro* transcribed labeled RNA fragments complementary to exon-intron regions in each transcript. DNA fragments, amplified by PCR using a 5′ primer containing the T7 RNA polymerase promoter sequence fused to the gene of interest, were used to generate RNA probes (labeled with Fluorescein-12-UTP, Cat. 11427857910, Sigma-Aldrich Israel Ltd, Rehovot, Israel) complementary to organellar transcripts. Detection was carried out using the Molecular Dynamics Storm system, and analyzed by the ImageQuant software at the Center for Molecular Dynamics (HUJI, Jerusalem, Israel).

Enrichment of organellar membranes from wild type and mutant seedlings

Crude organellar membrane fractions from wild type and mutant plants were prepared as previously described (Pineau *et al.* 2008) with minor adjustments (Shevtsov *et al.* 2018). Approximately 200 mg of whole plant tissue was homogenized in 2.0 mL of membrane extraction

buffer (75 mM MOPS-KOH, pH 7.6; 0.6 M sucrose; 4 mM EDTA; 0.2% polyvinylpyrrolidone-40; 8 mM L-cysteine; and 0.2% bovine serum albumin). The homogenate was filtered through a single layer of Miracloth to remove cell debris and centrifuged at 1,300 × g to pellet cell fragments and thylakoid membranes. The crude mitochondrial fraction was collected by a sequential centrifugation at 22,000 ×g for 10 minutes at 4°C.

Analysis of the steady state levels of organellar proteins in wild type and mutant plants

Protein was extracted from crude organellar membrane fractions corresponding to approximately 200 mg of fresh whole-plant tissue, solubilized in protein sample buffer, and separated by SDS-PAGE (Laemmli 1970). For immunoblotting, the proteins were transferred onto a PVDF membrane and incubated overnight at 4°C with specific antibodies (Table S5). Detection was performed using chemiluminescence following incubation with horseradish peroxidase (HRP)-conjugated secondary antibody.

Blue Native (BN-) PAGE analysis of mitochondrial respiratory complexes

BN-PAGE of crude organellar membranous fractions was performed generally according to the method described by Pineau *et al.* (2008). In brief, crude organellar membrane fraction, equivalent of 200 mg MS-agar grown Arabidopsis seedlings, was solubilized in 200 µL of 1.5% (w/v) n-Dodecyl β-D-maltoside (DDM, CAS no. 69227-93-6) solution containing 0.6% (w/v) Brilliant Blue G (CAS no. 6104-58-1). Insoluble materials were removed by a centrifugation step (i.e., 20,000 xg). Solubilized membrane fractions were loaded onto a native gel. For immunoblotting, the proteins were transferred to a PVDF membrane, and incubated with primary antibodies (Table S5), as indicated in each blot. Detection was carried out by chemiluminescence assay with horseradish peroxidase (HRP)-conjugated secondary antibody.

Estimation of the relative accumulation of different organellar proteins in wild type (Col-0) and *ppr9* mutant plants

Detection of organellar proteins was performed by immunoblotting assays and using the ImageQuant™ LAS-4000 system (GE Healthcare Life Sciences, Daniel Biotech, Rehovot, Israel) following chemiluminescence assays with horseradish peroxidase (HRP)-conjugated secondary

antibodies. The signals were analyzed and quantified using the Fiji open-source software (Schindelin *et al.* 2012).

Data statement

The Arabidopsis Information Resource (TAIR) database provides genetic and molecular biology data for the model plant *Arabidopsis thaliana* (Reiser *et al.* 2024). The predicted three-dimensional structures of proteins were obtained from and analyzed using the AlphaFold Protein Structure Database, which provides publicly accessible computational models of protein structures (Varadi *et al.* 2023). Accession numbers: Arabidopsis mitochondrial genome, BK010421.1; PPR9: gene AT1G03560, protein Q9LR67 (PPR9_ARATH). Data supporting the results of this study can be obtained from the corresponding author upon reasonable request.

Acknowledgements

The authors thank Dr. Yoram Soroka and Dr. Haim Azulay (The Hebrew University of Jerusalem, Israel) for their assistance with mutant analyses. We also thank Prof. Dr. Ute Höcker (University of Cologne, Germany) for providing *P. patens* lines and protocols for protoplasts preparation and transformation. Confocal microscopy was assisted by Dr. Yang-Sung Sohn (HUJI) and supported by the 'Charles E. Smith Family' and the 'Prof. Joel Elkes Laboratory for Collaborative Research in Psychobiology' (HUJI). This work was supported by grants to O.O.B. from the Israel Science Foundation (ISF-911/25 and ISF-1834/20).

Short legends for Supporting Information

Table S1. PPR9 mt-RNA gene-loci binding predictions.

Table S2. Quantification data of protein profiles.

Table S3. List of oligonucleotides used for the screening of *ppr9* mutants in this study.

Table S4. List of RT-qPCR oligonucleotides designed to specific different exon-exon (analysis of mRNA and processed transcripts) and intron-exon regions (analysis of pre-RNAs) in Arabidopsis mitochondria.

Table S5. List of antibodies used for the analysis of organellar proteins in wild type and *ppr9* mutant plants.

Figure S1. PPR9 protein structure and its predicated RNA biding site.

Figure S2. Expression patterns of PPR9 across tissues and developmental stages.

Figure S3. Developmental phenotypes associated with embryo-rescued *ppr9* mutants.

Figure S4. mt-RNA metabolism defects associated with embryo-rescued *ppr9* mutants.

Author contributions statement

E.K. and M.K. performed plant growth and analyses, established embryo-rescued mutant lines, and conducted DNA, RNA, and protein analyses. R. Ma. carried out GFP localization experiments. R. Mi. assisted with protein folding analyses and RNase protection assays. N.C. conducted *in silico* predictions of PPR9 RNA targets. O.O.B. served as principal investigator, supervised the project, and prepared the manuscript as the corresponding author.

References

Barkan, A., Rojas, M., Fujii, S., Yap, A., Chong, Y., Bond, C. and Small, I. (2012) A combinatorial amino acid code for RNA recognition by pentatricopeptide repeat proteins. *PLoS Genet*, **8**, e1002910.

Barkan, A. and Small, I. (2014) Pentatricopeptide repeat proteins in plants. *Annu Rev Plant Biol*, **65**, 415-442.

Best, C., Mizrahi, R., Edris, R., Tang, H., Zer, H., Colas des Francs-Small, C., Finkel, O.M., Zhu, H., Small, I.D. and Ostersetzer-Biran, O. (2023) MSP1 encodes an essential RNA-binding pentatricopeptide repeat factor required for nad1 maturation and complex I biogenesis in Arabidopsis mitochondria. *New Phytol*, **238**, 2375-2392.

Best, C., Mizrahi, R. and Ostersetzer-Biran, O. (2020a) Why so complex? The intricacy of genome structure and gene expression, associated with angiosperm mitochondria, may relate to the regulation of embryo quiescence or dormancy - intrinsic blocks to early plant life. *Plants*, **9**, 598-616.

Best, C., Sultan, L., Murik, O. and Ostersetzer-Biran, O. (2020b) Insights into the mitochondrial transcriptome landscapes of two Brassicales plant species, *Arabidopsis thaliana* (var. Col-0) and *Brassica oleracea* (var. botrytis). *Endocytobiosis Cell Res*, **30**, 16-38.

Bonen, L. (2008) Cis- and trans-splicing of group II introns in plant mitochondria. *Mitochondrion*, **8**, 26-34.

Boyes, D.C., Zayed, A.M., Ascenzi, R., McCaskill, A.J., Hoffman, N.E., Davis, K.R. and Görlach, J. (2001) Growth stage–based phenotypic analysis of Arabidopsis. A model for high throughput functional genomics in plants. *Plant cell*, **13**, 1499-1510.

Braun, H.-P. (2020) The Oxidative Phosphorylation system of the mitochondria in plants. *Mitochondrion*, **53**, 66-75.

Braun, H.-P., Binder, S., Brennicke, A., Eubel, H., Fernie, A.R., Finkemeier, I., Klodmann, J., König, A.-C., Kühn, K., Meyer, E., Obata, T., Schwarzländer, M., Takenaka, M. and Zehrmann, A. (2014) The life of plant mitochondrial complex I. *Mitochondrion*, **19**, 295-313.

Brown, G.G., Colas des Francs-Small, C. and Ostersetzer-Biran, O. (2014) Group II intron splicing factors in plant mitochondria. *Front Plant Sci*, **5**, 1-13.

Broz, A.K., Hodous, M.M., Zou, Y., Vail, P.C., Wu, Z. and Sloan, D.B. (2025) Flipping the switch on some of the slowest mutating genomes: Direct measurements of plant mitochondrial and plastid mutation rates in msh1 mutants. *PLOS Genetics*, **21**, e1011764.

Castandet, B., Choury, D., Begu, D., Jordana, X. and Araya, A. (2010) Intron RNA editing is essential for splicing in plant mitochondria. *Nucleic Acids Res*, **38**, 7112-7121.

Charlot, F., Goudounet, G., Nogué, F. and Perroud, P.-F. (2022) Physcomitrium patens Protoplasting and Protoplast Transfection. In *Protoplast Technology: Methods and Protocols* (Wang, K. and Zhang, F. eds). New York, NY: Springer US, pp. 3-19.

Cheng, S., Gutmann, B., Zhong, X., Ye, Y., Fisher, M.F., Bai, F., Castleden, I., Song, Y., Song, B., Huang, J., Liu, X., Xu, X., Lim, B.L., Bond, C.S., Yiu, S.M. and Small, I. (2016) Redefining the structural motifs that determine RNA binding and RNA editing by pentatricopeptide repeat proteins in land plants. *Plant J*, **85**, 532-547.

Cohen, S., Zmudjak, M., Colas des Francs-Small, C., Malik, S., Shaya, F., Keren, I., Belausov, E., Many, Y., Brown, G.G., Small, I. and Ostersetzer-Biran, O. (2014) nMAT4, a maturase factor required for *nad1* pre-mRNA processing and maturation, is essential for holocomplex I biogenesis in Arabidopsis mitochondria. *Plant J*, **78**, 253-268.

Colas des Francs-Small, C. and Small, I. (2014) Surrogate mutants for studying mitochondrially encoded functions. *Biochimie*, **100**, 234-242.

Cordoba, J.P., Marchetti, F., Soto, D., Martin, M.V., Pagnussat, G.C. and Zabaleta, E. (2016) The CA domain of the respiratory complex I is required for normal embryogenesis in Arabidopsis thaliana. *J Exp Bot*, **67**, 1589-1603.

Dahan, J., Tcherkez, G., Macherel, D., Benamar, A., Belcram, K., Quadrado, M., Arnal, N. and Mireau, H. (2014) Disruption of the CYTOCHROME C OXIDASE DEFICIENT1 gene leads to cytochrome c oxidase depletion and reorchestrated respiratory metabolism in Arabidopsis. *Plant Physiol*, **166**, 1788-1802.

Emanuelsson, O., Nielsen, H., Brunak, S. and Heijne, G.v. (2000) Predicting subcellular localization of proteins based on their N-terminal amino acid sequence. *J Mol Biol*, **300**, 1005-1016.

Falcon de Longevialle, A., Meyer, E.H., Andres, C., Taylor, N.L., Lurin, C., Millar, A.H. and Small, I.D. (2007) The pentatricopeptide repeat gene OTP43 is required for *trans*-splicing of the mitochondrial *nad1* intron 1 in *Arabidopsis thaliana*. *Plant cell*, **19**, 3256-3265.

Farre, J.C., Aknin, C., Araya, A. and Castandet, B. (2012) RNA editing in mitochondrial trans-introns is required for splicing. *PLoS ONE*, **7**, e52644.

Formosa, L.E., Dibley, M.G., Stroud, D.A. and Ryan, M.T. (2018) Building a complex complex: Assembly of mitochondrial respiratory chain complex I. *Semin Cell Dev Biol*, **76**, 154-162.

Franzmann, L., Patton, D.A. and Meinke, D.W. (1989) In vitro morphogenesis of arrested embryos from lethal mutants of *Arabidopsis thaliana*. *Theor Appl Genet*, **77**, 609-616.

Fromm, S., Going, J., Lorenz, C., Peterhansel, C. and Braun, H.P. (2016) Depletion of the "gamma-type carbonic anhydrase-like" subunits of complex I affects central mitochondrial metabolism in *Arabidopsis thaliana*. *Biochim Biophys Acta*, **1857**, 60-71.

Fuchs, P., Rugen, N., Carrie, C., Elsasser, M., Finkemeier, I., Giese, J., Hildebrandt, T.M., Kuhn, K., Maurino, V.G., Ruberti, C., Schallenberg-Rudinger, M., Steinbeck, J., Braun, H.P., Eubel, H., Meyer, E.H., Muller-Schussele, S.J. and Schwarzlander, M. (2020) Single organelle function and organization as estimated from Arabidopsis mitochondrial proteomics. *Plant J*, **101**, 420-441.

Grüttner, S., Nguyen, T.-T., Bruhs, A., Mireau, H. and Kempken, F. (2022) The P-type pentatricopeptide repeat protein DWEORG1 is a non-previously reported rPPR protein of Arabidopsis mitochondria. *Scientific Reports*, **12**, 12492.

Gualberto, J.M. and Newton, K.J. (2017) Plant mitochondrial genomes: Dynamics and mechanisms of mutation. *Annu Rev Plant Biol*, **68**, 225-252.

Guerrero-Castillo, S., Baertling, F., Kownatzki, D., Wessels, H.J., Arnold, S., Brandt, U. and Nijtmans, L. (2017) The assembly pathway of mitochondrial respiratory chain Complex I. *Cell metabolism*, **25**, 128-139.

Gully, B.S., Cowieson, N., Stanley, W.A., Shearston, K., Small, I.D., Barkan, A. and Bond, C.S. (2015a) The solution structure of the pentatricopeptide repeat protein PPR10 upon binding atpH RNA. *Nucleic Acids Res*, **43**, 1918-1926.

Gully, B.S., Shah, K.R., Lee, M., Shearston, K., Smith, N.M., Sadowska, A., Blythe, A.J., Bernath-Levin, K., Stanley, W.A., Small, I.D. and Bond, C.S. (2015b) The design and structural characterization of a synthetic pentatricopeptide repeat protein. *Acta crystallographica. Section D, Biological crystallography*, **71**, 196-208.

Gutmann, B., Royan, S., Schallenberg-Rüdinger, M., Lenz, H., Castleden, I.R., McDowell, R., Vacher, M.A., Tonti-Filippini, J., Bond, C.S., Knoop, V. and Small, I.D. (2020) The expansion and diversification of pentatricopeptide repeat RNA-editing factors in plants. *Molecular plant*, **13**, 215-230.

Hammani, K. and Giege, P. (2014) RNA metabolism in plant mitochondria. *Trends Plant Sci*, **19**, 380-389.

Hooper, C.M., Castleden, I.R., Tanz, S.K., Aryamanesh, N. and Millar, A.H. (2017) SUBA4: the interactive data analysis centre for Arabidopsis subcellular protein locations. *Nucleic Acids Res*, **45**, D1064-D1074.

Huala, E., Dickerman, A.W., Garcia-Hernandez, M., Weems, D., Reiser, L., LaFond, F., Hanley, D., Kiphart, D., Zhuang, M., Huang, W., Mueller, L.A., Bhattacharyya, D., Bhaya, D., Sobral, B.W., Beavis, W., Meinke, D.W., Town, C.D., Somerville, C. and Rhee, S.Y. (2001) The Arabidopsis Information Resource (TAIR): a comprehensive database and web-based information retrieval, analysis, and visualization system for a model plant. *Nucleic Acids Res*, **29**, 102-105.

Huss, J.C. and Gierlinger, N. (2021) Functional packaging of seeds. *New Phytol*, **230**, 2154-2163.

Jumper, J., Evans, R., Pritzel, A., Green, T., Figurnov, M., Ronneberger, O., Tunyasuvunakool, K., Bates, R., Žídek, A., Potapenko, A., Bridgland, A., Meyer, C., Kohl, S.A.A., Ballard, A.J., Cowie, A., Romera-Paredes, B., Nikolov, S., Jain, R., Adler, J., Back, T., Petersen, S., Reiman, D., Clancy, E., Zielinski, M., Steinegger, M., Pacholska, M., Berghammer, T., Bodenstein, S., Silver, D., Vinyals, O., Senior, A.W., Kavukcuoglu, K., Kohli, P. and Hassabis, D. (2021) Highly accurate protein structure prediction with AlphaFold. *Nature*, **596**, 583-589.

Keren, I., Bezawork-Geleta, A., Kolton, M., Maayan, I., Belausov, E., Levy, M., Mett, A., Gidoni, D., Shaya, F. and Ostersetzer-Biran, O. (2009) AtnMat2, a nuclear-encoded maturase required for splicing of group-II introns in Arabidopsis mitochondria. *RNA*, **15**, 2299-2311.

Keren, I., Tal, L., Colas des Francs-Small, C., Araújo, W.L., Shevtsov, S., Shaya, F., Fernie, A.R., Small, I. and Ostersetzer-Biran, O. (2012) nMAT1, a nuclear-encoded maturase involved in the *trans*-splicing of *nad1* intron 1, is essential for mitochondrial complex I assembly and function. *Plant J*, **71**, 413-426.

Klusch, N., Dreimann, M., Senkler, J., Rugen, N., Kühlbrandt, W. and Braun, H.-P. (2023) Cryo-EM structure of the respiratory I + III2 supercomplex from *Arabidopsis thaliana* at 2 Å resolution. *Nature Plants*, **9**, 142-156.

Klusch, N., Senkler, J., Yildiz, Ö., Kühlbrandt, W. and Braun, H.-P. (2021) A ferredoxin bridge connects the two arms of plant mitochondrial complex I. *Plant cell*, **33**, 2072-2091.

Knoop, V. (2012) Seed plant mitochondrial genomes: Complexity evolving. In *Genomics of chloroplasts and mitochondria* (Bock, R. and Knoop, V. eds), pp. 175-200.

Kuhn, K., Obata, T., Feher, K., Bock, R., Fernie, A.R. and Meyer, E.H. (2015) Complete mitochondrial complex I deficiency induces an up-regulation of respiratory fluxes that is abolished by traces of functional complex I. *Plant Physiol*, **168**, 1537-1549.

Kwasniak-Owczarek, M., Kazmierczak, U., Tomal, A., Mackiewicz, P. and Janska, H. (2019) Deficiency of mitoribosomal S10 protein affects translation and splicing in Arabidopsis mitochondria. *Nucleic Acids Res*, **47**, 11790-11806.

Laemmli, U.K. (1970) Cleavage of structural proteins during the assembly of the head of bacteriophage T4. *Nature*, **227**, 680-685.

Lambowitz, A.M. and Belfort, M. (2015) Mobile bacterial group II introns at the crux of eukaryotic evolution. *Microbiology spectrum*, **3**, 1-26.

Lambowitz, A.M. and Zimmerly, S. (2011) Group II introns: mobile ribozymes that invade DNA. *Perspect Biol*, **3**, 1-19.

Lenz, H., Hein, A. and Knoop, V. (2018) Plant organelle RNA editing and its specificity factors: enhancements of analyses and new database features in PREPACT 3.0. *BMC bioinformatics*, **19**, 255-273.

Ligas, J., Pineau, E., Bock, R., Huynen, M.A. and Meyer, E.H. (2019) The assembly pathway of complex I in *Arabidopsis thaliana*. *Plant J*, **97**, 447-459.

Liu, Y., He, J., Chen, Z., Ren, X., Hong, X. and Gong, Z. (2010) ABA overly-sensitive 5 (ABO5), encoding a pentatricopeptide repeat protein required for cis-splicing of mitochondrial nad2 intron 3, is involved in the abscisic acid response in Arabidopsis. *Plant J*, **63**, 749-765.

Luna-García, V., Bernal Gallardo, J.J., Rethoret-Pasty, M., Pasha, A., Provart, N.J. and de Folter, S. (2023) A high-resolution gene expression map of the medial and lateral domains of the gynoecium of Arabidopsis. *Plant Physiol*, **195**, 410-429.

Maldonado, M., Padavannil, A., Zhou, L., Guo, F. and Letts, J.A. (2020) Atomic structure of a mitochondrial complex I intermediate from vascular plants. *eLife*, **9**, e56664.

Meyer, E.H., Welchen, E. and Carrie, C. (2019) Assembly of the complexes of the Oxidative Phosphorylation system in land plant mitochondria. *Annu Rev Plant Biol*, **70**, 23-50.

Millar, A.H., Whelan, J., Soole, K.L. and Day, D.A. (2011) Organization and regulation of mitochondrial respiration in plants. *Ann Rev Plant Biol*, **62**, 79-104.

Mizrahi, R. and Ostersetzer-Biran, O. (2024) Mitochondrial RNA helicases: key players in the regulation of plant organellar RNA splicing and gene expression. *Int J Mol Sci*, **25**, 5502.

Mizrahi, R., Shevtsov-Tal, S. and Ostersetzer-Biran, O. (2022) Group II intron-encoded proteins (IEPs/maturases) as key regulators of Nad1 expression and Complex I biogenesis in land plant mitochondria. *Genes*, **13**, 1-16.

Møller, I.M., Rasmusson, A.G. and Van Aken, O. (2021) Plant mitochondria – past, present and future. *Plant J*, **108**, 912-959.

Nguyen, T.-T., Best, C., Shevtsov, S., Zmudjak, M., Quadrado, M., Mizrahi, R., Zer, H., Mireau, H. and Ostersetzer-Biran, O. (2022) MISF2 encodes an essential mitochondrial splicing cofactor required for *nad2* mRNA processing and embryo development in *Arabidopsis thaliana*. *Int J Mol Sci*, **23**, 2670.

O'Toole, N., Hattori, M., Andres, C., Iida, K., Lurin, C., Schmitz-Linneweber, C., Sugita, M. and Small, I. (2008) On the expansion of the pentatricopeptide repeat gene family in plants. *Mol Biol Evol*, **25**, 1120-1128.

Ostersetzer-Biran, O. (2016) Respiratory complex I and embryo development. *J Exp Bot*, **67**, 1205-1207.

Ostersetzer, O., Cooke, A.M., Watkins, K.P. and Barkan, A. (2005) CRS1, a chloroplast group II Intron splicing factor, promotes intron folding through specific interactions with two intron domains. *Plant cell*, **17**, 241-255.

Pineau, B., Layoune, O., Danon, A. and De Paepe, R. (2008) L-galactono-1,4-lactone dehydrogenase is required for the accumulation of plant respiratory complex I. *J Biol Chem*, **283**, 32500-32505.

Pinfield-Wells, H., Rylott, E.L., Gilday, A.D., Graham, S., Job, K., Larson, T.R. and Graham, I.A. (2005) Sucrose rescues seedling establishment but not germination of Arabidopsis mutants disrupted in peroxisomal fatty acid catabolism. *Plant J*, **43**, 861-872.

Reiser, L., Bakker, E., Subramaniam, S., Chen, X., Sawant, S., Khosa, K., Prithvi, T. and Berardini, T.Z. (2024) The Arabidopsis Information Resource in 2024. *Genetics*, **227**, 1-11.

Rovira, A.G. and Smith, A.G. (2019) PPR proteins - orchestrators of organelle RNA metabolism. *Physiol Plant*, **166**, 451-459.

Rugen, N., Senkler, M. and Braun, H.P. (2024) Deep proteomics reveals incorporation of unedited proteins into mitochondrial protein complexes in Arabidopsis. *Plant Physiol*, **195**, 1180-1199.

Rugen, N., Straube, H., Franken, L.E., Braun, H.P. and Eubel, H. (2019) Complexome profiling reveals association of PPR proteins with ribosomes in the mitochondria of plants. *Mol Cell Proteomics*, **18**, 1345-1362.

Russell, R., Jarmoskaite, I. and Lambowitz, A.M. (2013) Toward a molecular understanding of RNA remodeling by DEAD-box proteins. *RNA biology*, **10**, 44-55.

Schaefer, D., Zryd, J.P., Knight, C.D. and Cove, D.J. (1991) Stable transformation of the moss Physcomitrella patens. *Molecular and General Genetics MGG*, **226**, 418-424.

Schallenberg-Rüdinger, M., Lenz, H., Polsakiewicz, M., Gott, J.M. and Knoop, V. (2013) A survey of PPR proteins identifies DYW domains like those of land plant RNA editing factors in diverse eukaryotes. *RNA biology*, **10**, 1549-1556.

Schindelin, J., Arganda-Carreras, I., Frise, E., Kaynig, V., Longair, M., Pietzsch, T., Preibisch, S., Rueden, C., Saalfeld, S., Schmid, B., Tinevez, J.-Y., White, D.J., Hartenstein, V., Eliceiri, K.,

Tomancak, P. and Cardona, A. (2012) Fiji: an open-source platform for biological-image analysis. *Nature methods*, **9**, 676-682.

Schmitz-Linneweber, C., Lampe, M.-K., Sultan, L.D. and Ostersetzer-Biran, O. (2015) Organellar maturases: A window into the evolution of the spliceosome. *BBA - Bioenergetics*, **1847**, 798-808.

Schmitz-Linneweber, C. and Small, I. (2008) Pentatricopeptide repeat proteins: a socket set for organelle gene expression. *Trends Plant Sci*, **13**, 663-670.

Senkler, J., Senkler, M., Eubel, H., Hildebrandt, T., Lengwenus, C., Schertl, P., Schwarzländer, M., Wagner, S., Wittig, I. and Braun, H.-P. (2017) The mitochondrial complexome of *Arabidopsis thaliana*. *Plant J*, **89**, 1079-1092.

Shen, C., Wang, X., Liu, Y., Li, Q., Yang, Z., Yan, N., Zou, T. and Yin, P. (2015) Specific RNA recognition by designer pentatricopeptide repeat protein. *Molecular plant*, **8**, 667-670.

Shen, C., Zhang, D., Guan, Z., Liu, Y., Yang, Z., Yang, Y., Wang, X., Wang, Q., Zhang, Q., Fan, S., Zou, T. and Yin, P. (2016) Structural basis for specific single-stranded RNA recognition by designer pentatricopeptide repeat proteins. *Nature Communications*, **7**, 11285.

Shevtsov-Tal, S., Best, C., Matan, R., Chandran, S.A., Brown, G.G. and Ostersetzer-Biran, O. (2021) nMAT3 is an essential maturase splicing factor required for holo-complex I biogenesis and embryo development in *Arabidopsis thaliana* plants. *Plant J*, **106**, 1128-1147.

Shevtsov, S., Nevo-Dinur, K., Faigon, L., Sultan, L.D., Zmudjak, M., Markovits, M. and Ostersetzer-Biran, O. (2018) Control of organelle gene expression by the mitochondrial transcription termination factor mTERF22 in *Arabidopsis thaliana* plants. *PLOS ONE*, **13**, e0201631.

Sloan, D.B., Wu, Z. and Sharbrough, J. (2018) Correction of persistent errors in Arabidopsis reference mitochondrial genomes. *Plant cell*, **30**, 525-527.

Small, I., Melonek, J., Bohne, A.-V., Nickelsen, J. and Schmitz-Linneweber, C. (2023) Plant organellar RNA maturation. *Plant cell*, **35**, 1727-1751.

Small, I.D. and Peeters, N. (2000) The PPR motif - a TPR-related motif prevalent in plant organellar proteins. *Trends Biochem Sci*, **25**, 46-47.

Small, I.D., Schallenberg-Rudinger, M., Takenaka, M., Mireau, H. and Ostersetzer-Biran, O. (2020) Plant organellar RNA editing: what 30 years of research has revealed. *Plant J*, **101**, 1040-1056.

Soufari, H., Parrot, C., Kuhn, L., Waltz, F. and Hashem, Y. (2020) Specific features and assembly of the plant mitochondrial complex I revealed by cryo-EM. *Nat Commun*, **11**, 5195.

Subrahmanian, N., Remacle, C. and Hamel, P.P. (2016) Plant mitochondrial complex I composition and assembly: A review. *BBA - Bioenergetics*, **1857**, 1001-1014.

Takenaka, M., Jorg, A., Burger, M. and Haag, S. (2019) RNA editing mutants as surrogates for mitochondrial SNP mutants. *Plant Physiol Biochem*, **135**, 310-321.

Takenaka, M., Zehrmann, A., Brennicke, A. and Graichen, K. (2013) Improved Computational Target Site Prediction for Pentatricopeptide Repeat RNA Editing Factors. *PLOS ONE*, **8**, e65343.

Thévenin, J., Dubos, C., Xu, W., Le Gourrierec, J., Kelemen, Z., Charlot, F., Nogué, F., Lepiniec, L. and Dubreucq, B. (2012) A new system for fast and quantitative analysis of heterologous gene expression in plants. *New Phytol*, **193**, 504-512.

Thévenin, J., Xu, W., Vaisman, L., Lepiniec, L., Dubreucq, B. and Dubos, C. (2016) The Physcomitrella patens System for Transient Gene Expression Assays. In *Plant Synthetic Promoters: Methods and Protocols* (Hehl, R. ed. New York, NY: Springer New York, pp. 151-161.

Varadi, M., Bertoni, D., Magana, P., Paramval, U., Pidruchna, I., Radhakrishnan, M., Tsenkov, M., Nair, S., Mirdita, M., Yeo, J., Kovalevskiy, O., Tunyasuvunakool, K., Laydon, A., Žídek, A., Tomlinson, H., Hariharan, D., Abrahamson, J., Green, T., Jumper, J., Birney, E., Steinegger, M., Hassabis, D. and Velankar, S. (2023) AlphaFold Protein Structure Database in 2024: providing structure coverage for over 214 million protein sequences. *Nucleic Acids Res*, **52**, D368-D375.

Waltz, F., Nguyen, T.T., Arrive, M., Bochler, A., Chicher, J., Hammann, P., Kuhn, L., Quadrado, M., Mireau, H., Hashem, Y. and Giege, P. (2019) Small is big in Arabidopsis mitochondrial ribosome. *Nat Plants*, **5**, 106-117.

Wang, J., Liu, S., Li, C., Wang, T., Zhang, P. and Chen, K. (2017) PnLRR-RLK27, a novel leucine-rich repeats receptor-like protein kinase from the Antarctic moss Pohlia nutans, positively regulates salinity and oxidation-stress tolerance. *PLOS ONE*, **12**, e0172869.

Wu, C.H., Apweiler, R., Bairoch, A., Natale, D.A., Barker, W.C., Boeckmann, B., Ferro, S., Gasteiger, E., Huang, H., Lopez, R., Magrane, M., Martin, M.J., Mazumder, R., O'Donovan, C., Redaschi, N. and Suzek, B. (2006) The Universal Protein Resource (UniProt): an expanding universe of protein information. *Nucleic Acids Res*, **34**, D187-191.

Yan, J., Yao, Y., Hong, S., Yang, Y., Shen, C., Zhang, Q., Zhang, D., Zou, T. and Yin, P. (2019) Delineation of pentatricopeptide repeat codes for target RNA prediction. *Nucleic Acids Res*, **47**, 3728-3738.

Zhao, C. and Pyle, A.M. (2017a) The group II intron maturase: a reverse transcriptase and splicing factor go hand in hand. *Curr Opin Struct Biol*, **47**, 30-39.

Zhao, C. and Pyle, A.M. (2017b) Structural Insights into the Mechanism of Group II Intron Splicing. *Trends Biochem Sci*, **42**, 470-482.

Zimmerly, S. and Semper, C. (2015) Evolution of group II introns. *Mobile DNA*, **6**, 1-19.

Zmudjak, M. and Ostersetzer-Biran, O. (2018) RNA Metabolism and Transcript Regulation. In *Annual Plant Reviews.* (Roberts, J.A. ed, pp. 143-184.

Figure legends

Figure 1. The *AT1G03560* gene-locus (*PPR9*) encodes a putative mitochondria-localized PPR protein.

(a) Schematic representation of the *PPR9* (*AT1G03560*, UniProt Q9LR67) gene structure. *In silico* analysis suggests the presence of 13 conserved P-class PPR motifs (P1-P13), as well as an additional putative PPR motif (P?) located near the N-terminus of the protein. Numbers correspond to amino acid residues not assigned to any defined motif. The predicted mitochondrial targeting signal (mTS) and the T-DNA insertion site in the SALK_004994 line (*ppr9-1*) within the PPR9 coding region is indicated above the gene structure figure.

(b) Prediction of the putative RNA-binding sites of PPR9. The fifth and last amino acids of each PPR repeat are shown below the corresponding motifs. The predicted RNA-binding sites for *nad2* intron 3 and *nad7* introns 1 and 2 (Table S1) are illustrated, with nucleotides colored as follows: U (light green), C (blue), G (orange), A (yellow), and non-matching or unassigned bases (white). The predicted RNA-binding code is indicated below the figure.

Figure 2. GFP localization analyses.

Protoplasts were prepared from *P. patens* plantlets grown on sterile MS medium and transformed with the pCAMBIA-1302 vector containing a GFP sequence fused in-frame to the N-terminal region (246 bp) of the PPR9 (AT1G03560) coding sequence, under the control of CaMV 35S promoter and a NOS terminator sequence at the 3′ end. The figure shows confocal PPR9-eGFP fluorescence (green, top left panel) and MitoTracker (red, top middle panel) signals, a GFP-MitoTracker overlay (top right panel), chlorophyll autofluorescence (purple, bottom left panel), merged fluorescence channels (bottom middle panel), and a bright-field images (grayscale, bottom right panel).

Figure 3. *ppr9* mutant phenotypes.

Mature siliques obtained from heterozygous *ppr9* (SALK-004994) mutant line.

(a) Seeds collected from mature siliques of wild type (Col-0) and heterozygous *ppr9* plants. Arrows indicate abnormal homozygous *ppr9* mutant seeds, which appear shrunken and darker.

(b) Representative images of green (heterozygous or wild type embryos) and white (homozygous *ppr9* embryos) seeds observed in immature siliques of heterozygous *ppr9* plants (left panel). The

morphology of embryos in green or white seeds (middle panel) were analyzed by differential interference contrast (Nomarski, DIC) microscopy (right panel).

(c) Embryo-rescue procedure. Seeds collected under sterile conditions from surface-sterilized immature siliques of Col-0 or heterozygous *ppr9* plants were sown on MS-agar plates supplemented with 3% sucrose and vitamins (*i*), and grown under standard growth-chamber conditions. 2-month-old *ppr9* and Col-0 plantlets (growth stage L6) transferred to liquid MS medium supplemented with 3% sucrose and vitamins (*ii*). Homozygous *ppr9* plants exhibit abnormal morphology and developmental phenotypes, often displaying a bushy-like appearance (*iii*, *iv*), similar to that reported for other mutants affected in mt-RNA metabolism (Best *et al.* 2023, Dahan *et al.* 2014, Shevtsov-Tal *et al.* 2021).

Figure 4. The accumulation of *nad2* and *nad7* transcripts relies on PPR9 in Arabidopsis mitochondria.

The accumulation of various mitochondrial mRNA transcripts was analyzed by RT-qPCR. Total RNA isolated from 3-week-old Col-0 plants, 2~3-month-old rescued *ppr9* mutant, *ppr9/PPR9* mutant plants, and plantlets obtained from Col-0 embryos at the torpedo stage, was reverse-transcribed, and the relative steady-state levels of cDNAs corresponding to the different organellar transcripts were estimated by qPCR with primers which specifically amplified specific organellar transcripts (Table S4). Histograms showing the relative mRNAs levels (i.e., log2 ratios) in rescued (a) homozygous *ppr9* or (b) *ppr9/PPR* plants, versus those of germinated embryos from wild type seeds. The values are means of nine RT-qPCRs corresponding to three biological replicates (error bars indicate one standard deviation), after normalization to the *GAPDH* (*AT1G13440*), *ACTIN2* (*AT3G18780*), *18S rRNA* (*AT3G41768*), and the mitochondrial *26S rRNA* (*rrn26*, *ATMG00020*) genes. Red asterisks indicate transcripts whose levels were significantly reduced in the mutant relative to the wild type control.

Figure 5. PPR9 is required for *nad2* intron 3 splicing and *nad7* transcript maturation in Arabidopsis mitochondria

Total RNA was extracted from whole seedlings of wild type (Col-0), *ppr9/PPR9* and homozygous *ppr9* mutant plants. The relative (steady-state) levels of individual mitochondrial transcripts were evaluated by RT-qPCR, with oligonucleotides that designed to amplify specific organellar exon-

exon or exon-intron regions (Table S4), using Col-0 RNA as the calibrator. For quantification, transcript levels were further normalized to various reference genes, including the *GAPDH* (*AT1G13440*), *ACTIN2* (*AT3G18780*), *18S rRNA* (*AT3G41768*), and the mitochondrial *26S rRNA* (*rrn26*, *ATMG00020*) genes. Splicing efficiencies of each of the 23 mitochondrial group II introns in *ppr9* (a) and functionally complemented *ppr9/PPR9* were assessed based on the relative pre-RNA to mRNA ratios in the mutant lines compared with those of wild type plants. The histograms show the $\log_2$ fold change of mRNA/pre-RNA levels in the *ppr9* lines relative to Col-0. Data represent mean values from three biological replicates, each analyzed in triplicate (nine reactions in total). Error bars represent one standard deviation.

Figure 6. Defects in mitochondrial respiratory complex I biogenesis in *ppr9* mutants

Accumulation of mitochondrial respiratory complexes in germinated embryos (at the torpedo stage) of wild type (Col-0), *ppr9/PPR9* and homozygous *ppr9* mutant plants. The abundance and assembly state of mitochondrial respiratory complexes were assessed by blue-native polyacrylamide gel electrophoresis (BN-PAGE) of crude organellar membrane preparations from Col-0 plants and ppr9 mutant lines. Following native electrophoresis, proteins were transferred to PVDF membranes and analyzed by immunoblotting using antibodies against various organellar protein subunits (Table S5), following chemiluminescence (ECL) assays and then recorded on an imaging system (ImageQuant LAS 4000, GE Healthcare, Haifa, Israel). Signal detection was performed by chemiluminescence. Arrows indicate the positions of the major native respiratory complexes, including NADH:ubiquinone oxidoreductase (CI; ~1,000 kDa), cytochrome bc_1 complex dimer (also called ubiquinol:cytochrome c oxidoreductase, or $CIII_2$; ~500 kDa), cytochrome c oxidase (CIV; ~220 kDa), and the ATP synthase enzymes (CV; ~660 kDa). The asterisk in the CA2 panel marks the ~850-kDa CI stable assembly intermediate (CI*), while additional lower-molecular-mass signals in the CA2 blot likely correspond to earlier CI-assembly intermediates (Ligas *et al.* 2019, Ostersetzer-Biran 2016).

Figure 7. Accumulation of various organellar proteins in wild type and *ppr9* plants.

Crude organellar (mitochondria-enriched) membrane fractions were isolated from wild type (Col-0), *ppr9/PPR9* and homozygous *ppr9* mutant plants. Equal amounts of protein were separated by SDS-PAGE and analyzed by immunoblotting with specific antibodies raised against representative

organellar proteins (Table S5). Signals were detected using chemiluminescence (ECL) and recorded on an imaging system.

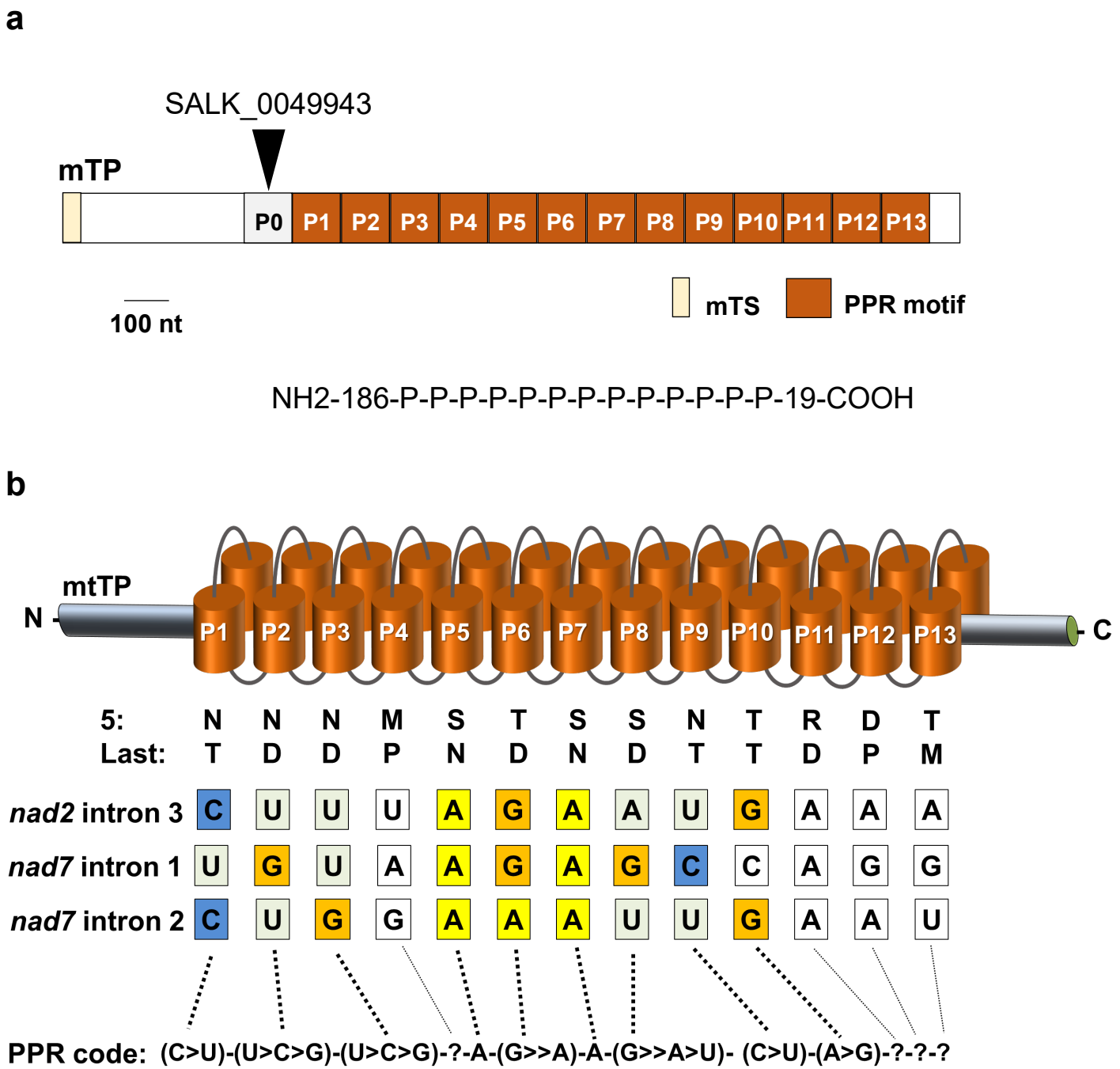
a
SALK_0049943
mTP
P0
P1
P2
P3
P4
P5
P6
P7
P8
P9
P10
P11
P12
P13
100 nt
mTS
PPR motif
NH2-186-P-P-P-P-P-P-P-P-P-P-P-P-P-19-COOH
b
mtTP
N
C
5: N N N M S T S S N T R D T
Last: T D D P N D N D T T D P M
nad2 intron 3 C U U U A G A A U G A A A
nad7 intron 1 U G U A A G A G C C A G G
nad7 intron 2 C U G G A A A U U G A A U
PPR code: (C>U)-(U>C>G)-(U>C>G)-?-A-(G>>A)-A-(G>>A>U)- (C>U)-(A>G)-?-?-?

Figure 1

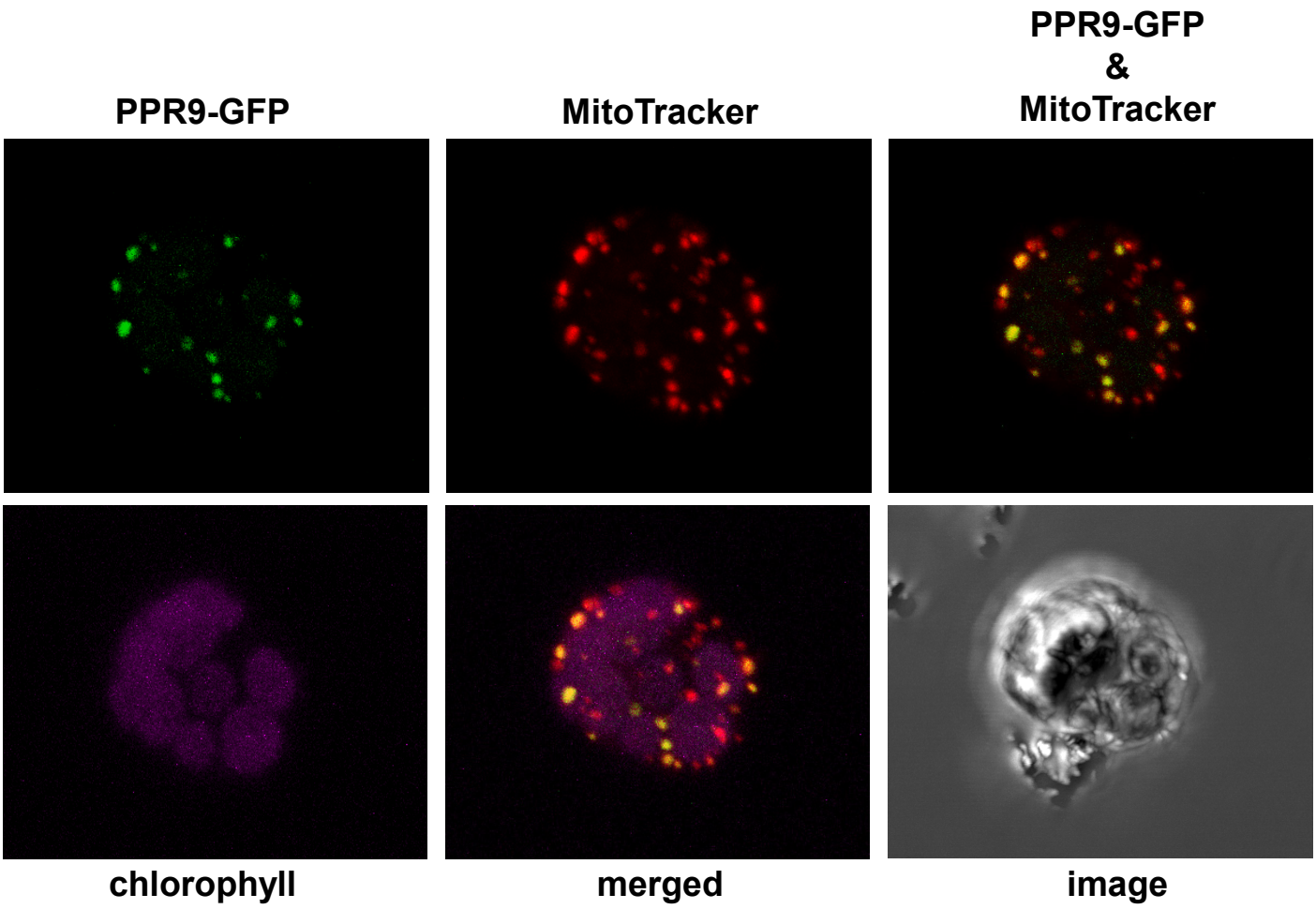
PPR9-GFP
MitoTracker
PPR9-GFP
&
MitoTracker
chlorophyll
merged
image

Figure 2

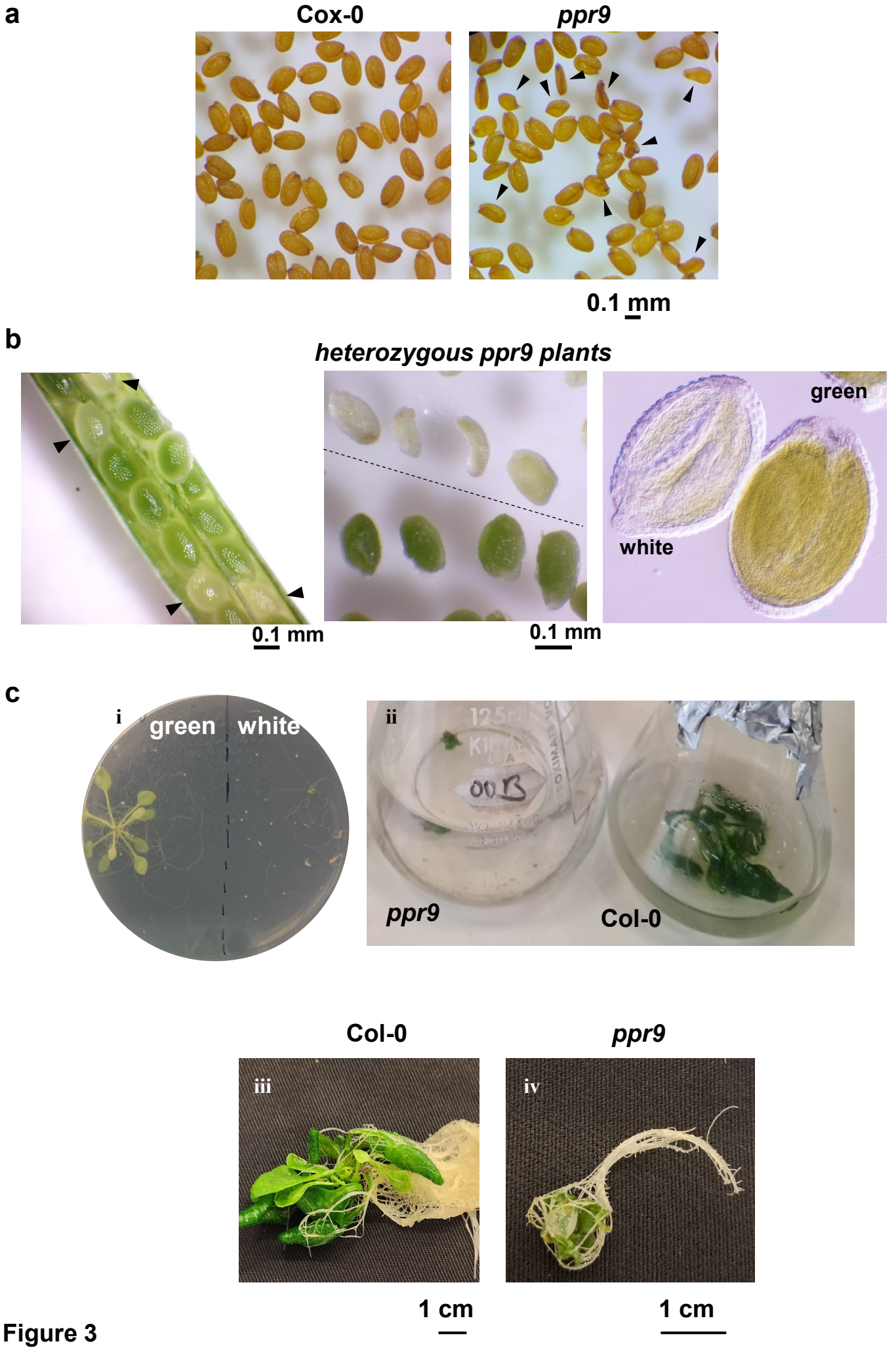
a
Cox-0
ppr9
0.1 mm
b
heterozygous ppr9 plants
green
white
0.1 mm
0.1 mm
c
i
green
white
ii
ppr9
Col-0
Col-0
ppr9
iii
iv
1 cm
1 cm

Figure 3

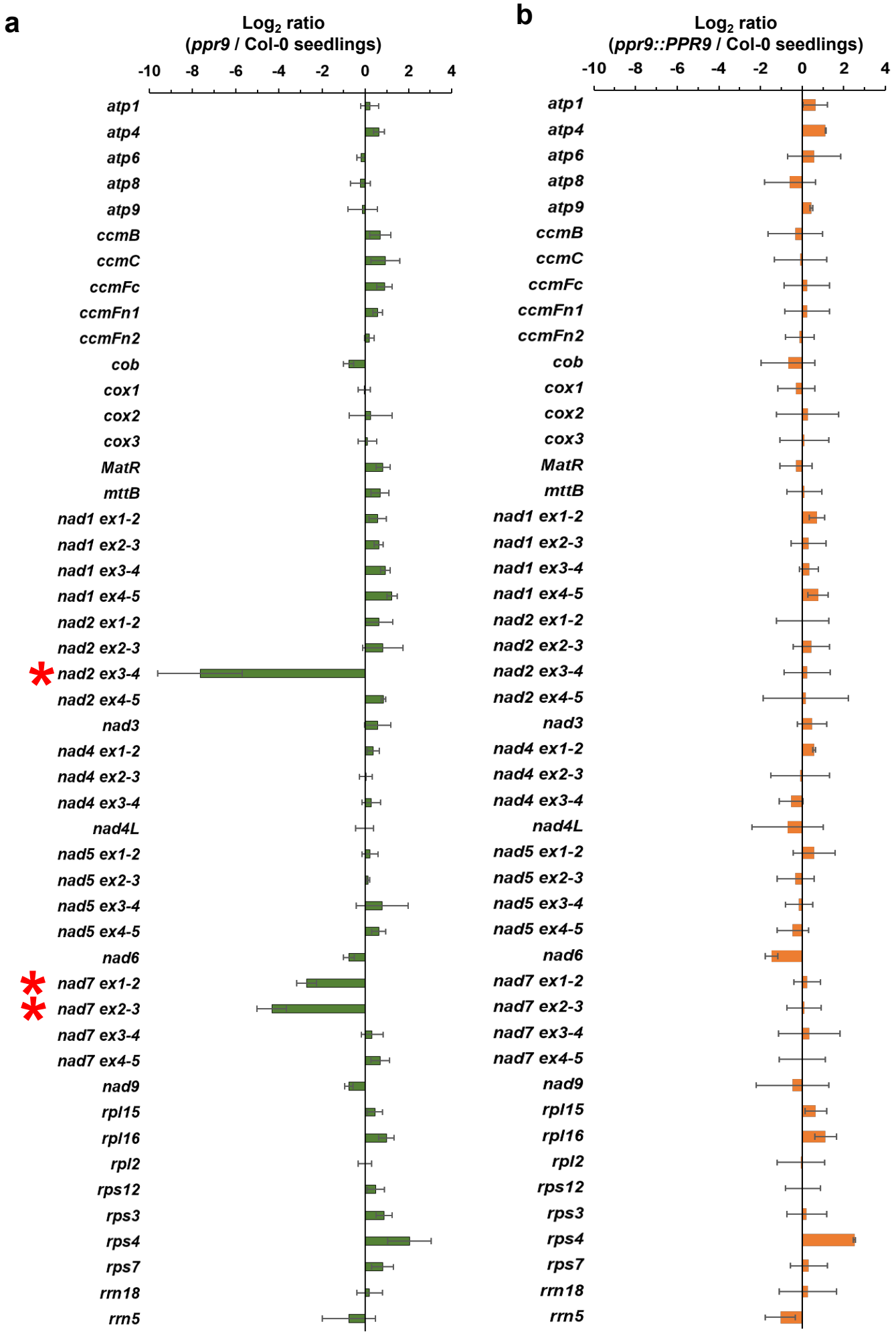
a
Log2 ratio
(ppr9 / Col-0 seedlings)
-10 -8 -6 -4 -2 0 2 4
atp1
atp4
atp6
atp8
atp9
ccmB
ccmC
ccmFc
ccmFn1
ccmFn2
cob
cox1
cox2
cox3
MatR
mttB
nad1 ex1-2
nad1 ex2-3
nad1 ex3-4
nad1 ex4-5
nad2 ex1-2
nad2 ex2-3
nad2 ex3-4
nad2 ex4-5
nad3
nad4 ex1-2
nad4 ex2-3
nad4 ex3-4
nad4L
nad5 ex1-2
nad5 ex2-3
nad5 ex3-4
nad5 ex4-5
nad6
nad7 ex1-2
nad7 ex2-3
nad7 ex3-4
nad7 ex4-5
nad9
rpl15
rpl16
rpl2
rps12
rps3
rps4
rps7
rrn18
rrn5
b
Log2 ratio
(ppr9::PPR9 / Col-0 seedlings)
-10 -8 -6 -4 -2 0 2 4
atp1
atp4
atp6
atp8
atp9
ccmB
ccmC
ccmFc
ccmFn1
ccmFn2
cob
cox1
cox2
cox3
MatR
mttB
nad1 ex1-2
nad1 ex2-3
nad1 ex3-4
nad1 ex4-5
nad2 ex1-2
nad2 ex2-3
nad2 ex3-4
nad2 ex4-5
nad3
nad4 ex1-2
nad4 ex2-3
nad4 ex3-4
nad4L
nad5 ex1-2
nad5 ex2-3
nad5 ex3-4
nad5 ex4-5
nad6
nad7 ex1-2
nad7 ex2-3
nad7 ex3-4
nad7 ex4-5
nad9
rpl15
rpl16
rpl2
rps12
rps3
rps4
rps7
rrn18
rrn5

Figure 4

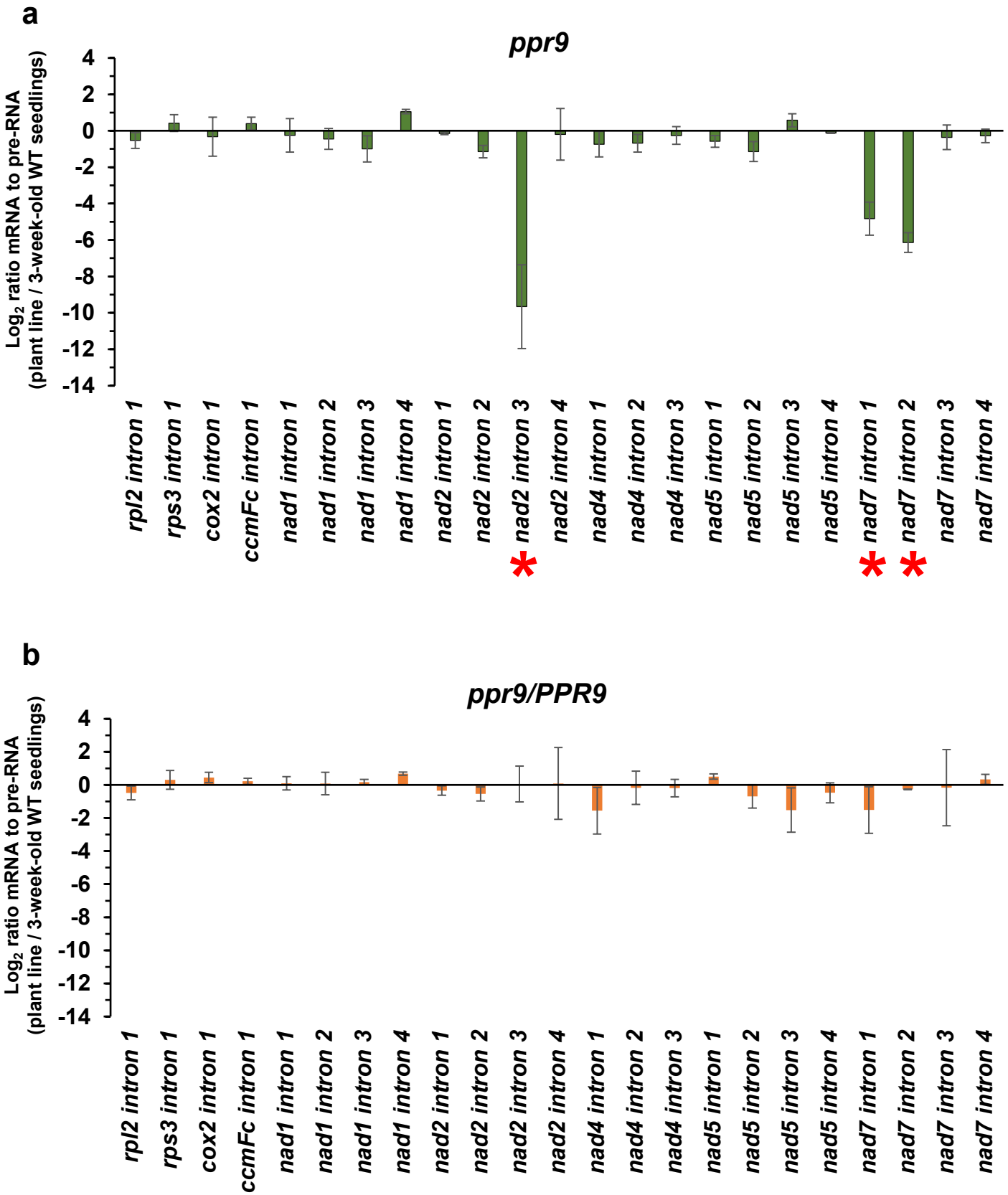
a
ppr9
Log2 ratio mRNA to pre-RNA
(plant line / 3-week-old WT seedlings)
4
2
0
-2
-4
-6
-8
-10
-12
-14
rpl2 intron 1
rps3 intron 1
cox2 intron 1
ccmFc intron 1
nad1 intron 1
nad1 intron 2
nad1 intron 3
nad1 intron 4
nad2 intron 1
nad2 intron 2
nad2 intron 3
nad2 intron 4
nad4 intron 1
nad4 intron 2
nad4 intron 3
nad5 intron 1
nad5 intron 2
nad5 intron 3
nad5 intron 4
nad7 intron 1
nad7 intron 2
nad7 intron 3
nad7 intron 4
*
*
*
b
ppr9/PPR9
Log2 ratio mRNA to pre-RNA
(plant line / 3-week-old WT seedlings)
4
2
0
-2
-4
-6
-8
-10
-12
-14
rpl2 intron 1
rps3 intron 1
cox2 intron 1
ccmFc intron 1
nad1 intron 1
nad1 intron 2
nad1 intron 3
nad1 intron 4
nad2 intron 1
nad2 intron 2
nad2 intron 3
nad2 intron 4
nad4 intron 1
nad4 intron 2
nad4 intron 3
nad5 intron 1
nad5 intron 2
nad5 intron 3
nad5 intron 4
nad7 intron 1
nad7 intron 2
nad7 intron 3
nad7 intron 4

Figure 5

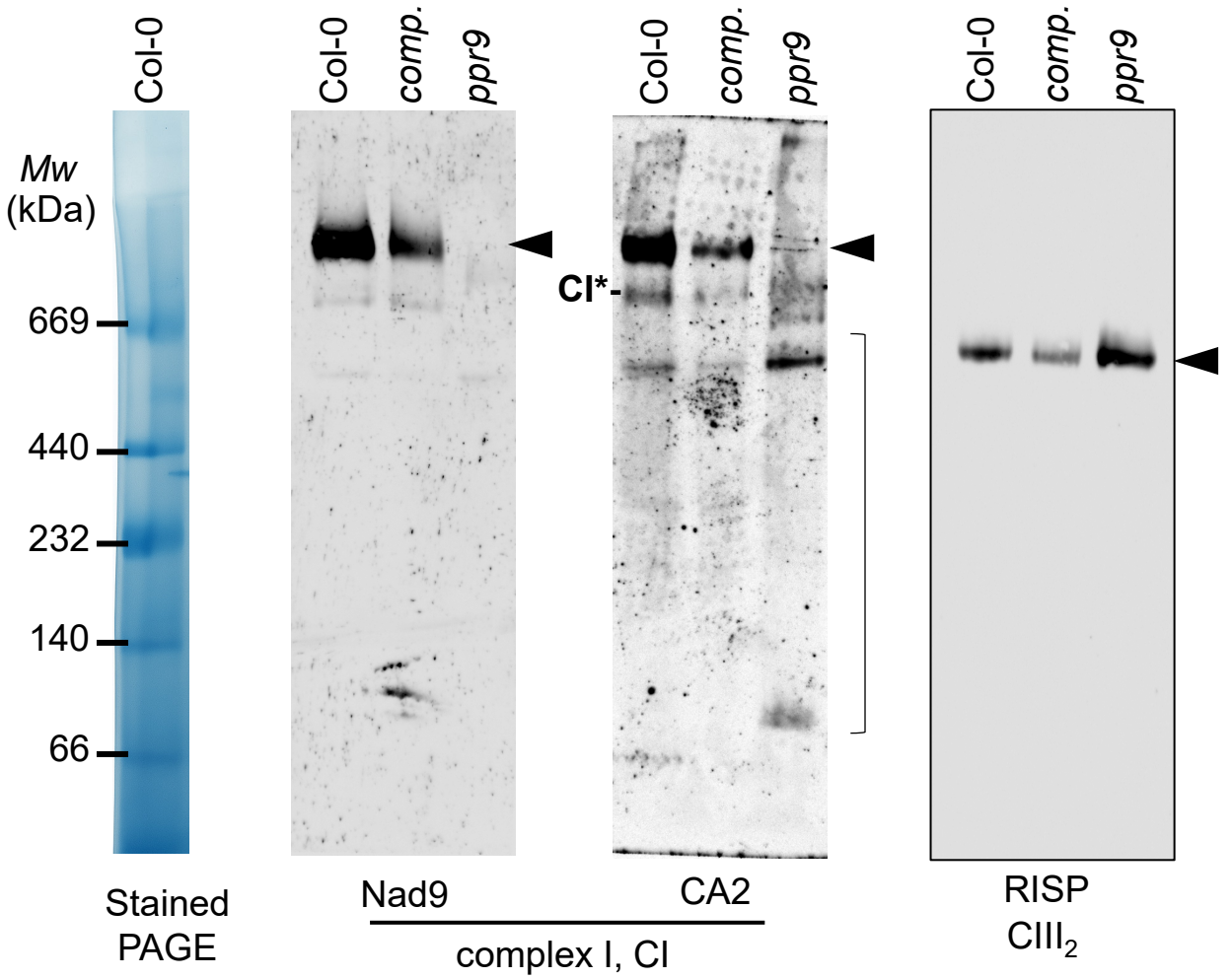
Col-0
Col-0
comp.
ppr9
Col-0
comp.
ppr9
Col-0
comp.
ppr9
Mw
(kDa)
669
440
232
140
66
CI*-
Stained
PAGE
Nad9
CA2
complex I, CI
RISP
CIII2

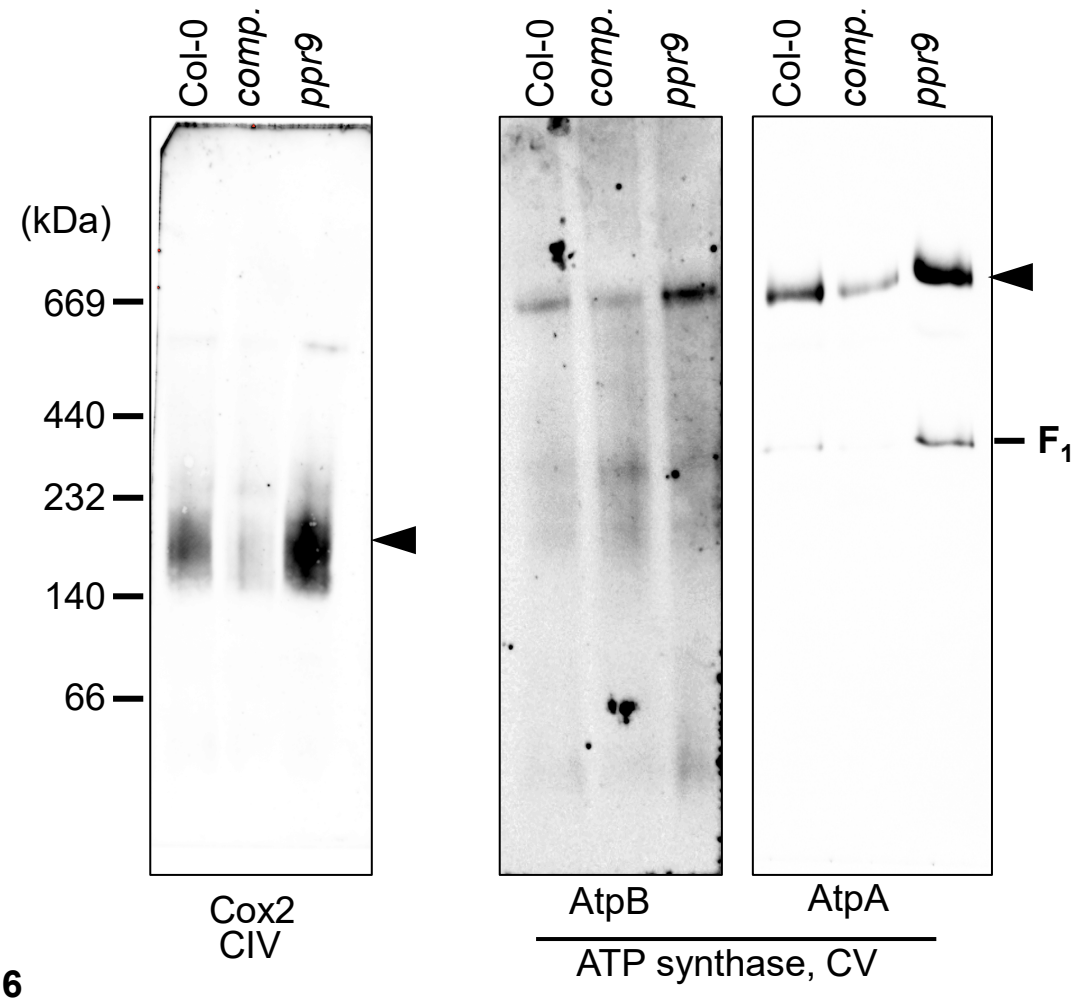
Col-0
comp.
ppr9
Col-0
comp.
ppr9
Col-0
comp.
ppr9
(kDa)
669
440
232
140
66
F1
Cox2
CIV
AtpB
AtpA
ATP synthase, CV

Figure 6

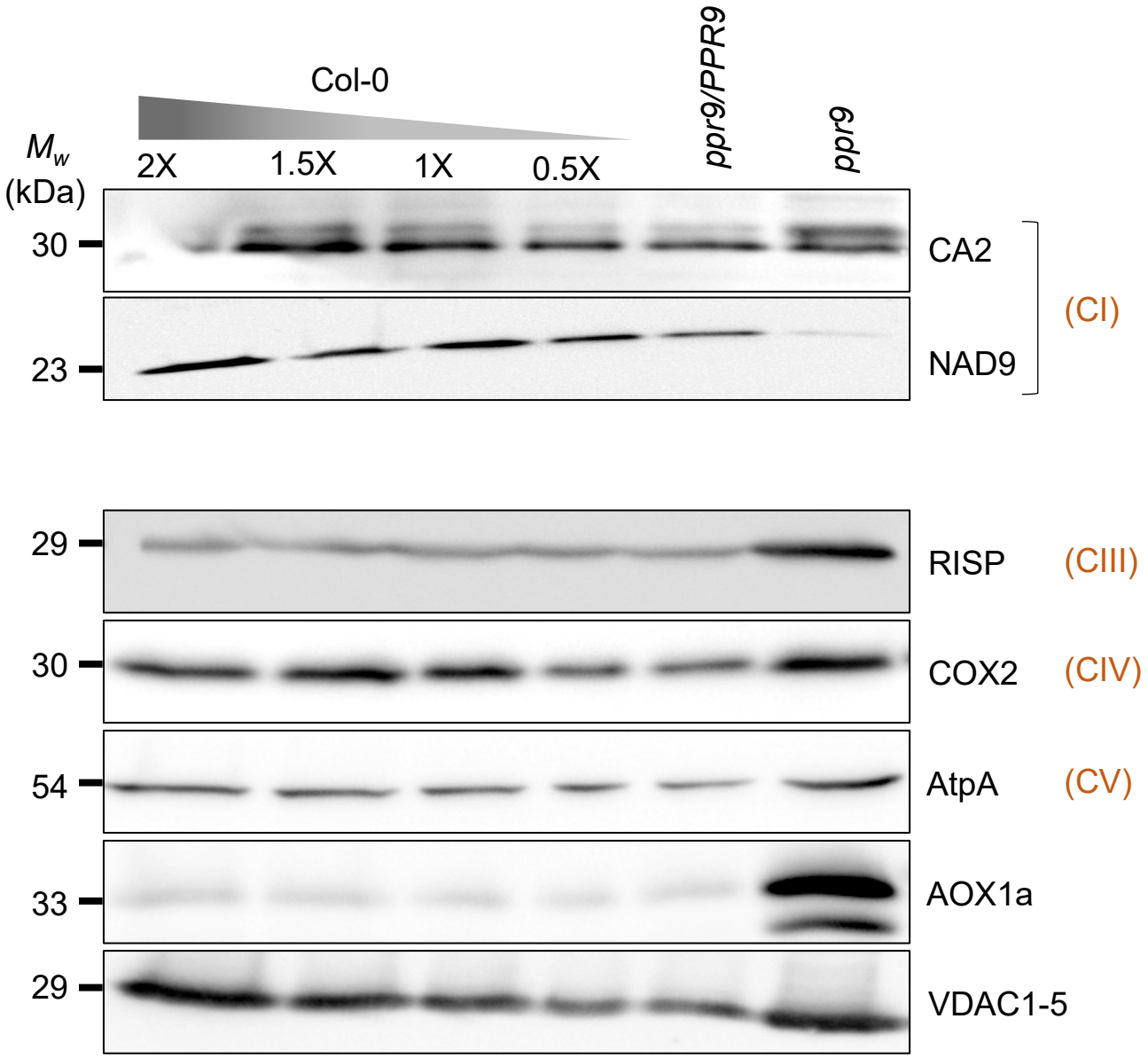
Col-0
2X
1.5X
1X
0.5X
ppr9/PPR9
ppr9
M_w
(kDa)
30
23
CA2
NAD9
(CI)
29
RISP
(CIII)
30
COX2
(CIV)
54
AtpA
(CV)
33
AOX1a
29
VDAC1-5

Figure 7